Searches for effects beyond the Standard Model in semileptonic B hadron decays at LHCb

Thesis defense

Bogdan KUTSENKO

Jury members:
Marie-Hélène Schune (Rapporteure)
Martin Jung (Rapporteur)
Michel De Cian (Examinateur)
Eric Kajfasz (Président du jury)

Supervisors:
Anton Poluektov (Directeur de thèse)
Dorothea vom Bruch (Codirectrice de thèse)

PhD defense – 24 September 2025

Content

The Standard Model of Particle Physics

Core Concepts

- Quantum Fields: particles are excitations of the fields
- Matter: 12 fermions (6 quarks in 6 **flavours**, 6 leptons in 3 **flavours**)
- Forces: 4 gauge bosons mediate interactions
- Higgs Boson: gives mass to particles

Achievements

- Predicted W, Z, Higgs, top quark
- Validated by precision experiments
- Unified 3 of 4 fundamental forces
- ...

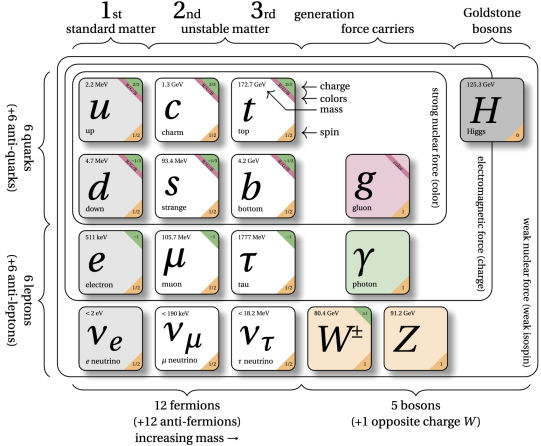

Standard Model: Open Problems and Searches for New Physics

Open Problems

- Gravity not included
- Cosmological Observations : Dark matter & dark energy
- Matter–antimatter asymmetry
- Neutrino masses & oscillations
- Hierarchy problem (EW vs. Planck scale)
- Strong CP problem
- Fermion mass hierarchy

Searches for New Physics

- **Direct:** heavy new particles at colliders
- **Indirect:** Probe deviations from SM predictions
  - Flavour physics approach (this thesis)

Effective Field Theory: Impact of New Physics at Scale Λ

- **Systematic, model-independent (within low-energy assumption) strategy is essential** $\rightarrow$ Effective Field Theory (EFT)
- Physics P with scale Λ
  - Λ can be a mass, confinement scale, etc.
  - At $E \ll \Lambda$: P states not produced on–shell (only internal lines)
- P effects at $E \ll \Lambda$:
  - Local operators, suppressed as $1/\Lambda^n$
  - Taylor expansion in E/Λ
  - For small E/Λ, P sector decouples

SMEFT Expansion:

$$\mathcal{L}_{\text{SMEFT}} = \mathcal{L}_{\text{SM}} + \frac{1}{\Lambda}\mathcal{L}_5 + \frac{1}{\Lambda^2}\mathcal{L}_6 + \frac{1}{\Lambda^3}\mathcal{L}_7 + \frac{1}{\Lambda^4}\mathcal{L}_8 + \ldots$$

$$\mathcal{L}_d = \sum_i C_i \, O_i^{(d)}$$

- C_i: Wilson coefficients (free parameters)
- O_i: Invariant operators of dimension d

Effective field theory

- Decay under study: $B^0 \to D^* \ell \nu_\ell$, where $\ell = e, \mu$
- The dimension-six EFT for $B^0 \to D^* \ell \nu_\ell$, assuming three light left-handed neutrino flavours below the electroweak scale :

- $\mathcal{L}_{eff}(b \to c\ell) = \frac{4G_F}{\sqrt{2}} V_{cb} \sum_i (\mathcal{O}_{SM} + C_i \mathcal{O}_i)$
  - Dominant SM. NP corrections parametrized by adding new operators and coefficients

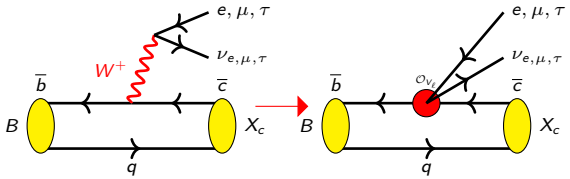

$$\mathcal{L}_{eff} = \frac{4G_F}{\sqrt{2}} V_{cb} \{ \left[(1 + C_{V_L}) P_L + C_{V_R} P_R \right] \gamma_\mu P_L + \left[C_S + C_P \gamma^5 \right] P_L + C_T \, \sigma^{\mu\nu} P_L \sigma_{\mu\nu} P_L + h.c. \}$$

- $C_{V_L}, C_{V_R}, C_S, C_P, C_T$ are complex NP couplings ($\equiv 0$ in SM)
- Different NP models (W', H^+, LQ, ...) $\Rightarrow$ different combinations of couplings

Lepton Flavour Universality

- Semileptonic b-hadron decays provide powerful probes for testing the

  Lepton Flavor Universality,

  electroweak boson interactions are lepton-flavour independent (e, μ, τ)

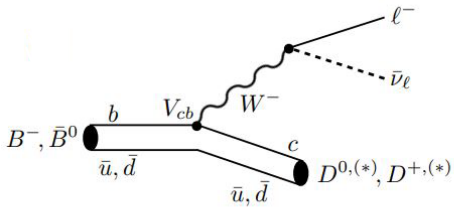

- LFU can be tested with ratios of branching fractions to final states with different lepton flavours:

$$R(D^{(*)})_{\tau/\ell} = \frac{Br(B^0 \to D^{(*)}\tau\nu_\tau)}{Br(B^0 \to D^{(*)}\ell\nu_\ell)},$$

  - The ratio reduces some theoretical uncertainties
  - NP may be more sensitive to the third generation

World Average of $R(D)$ and $R(D^*)$

World Averages

$$R(D) = 0.347 \pm 0.025$$

$$R(D^*) = 0.288 \pm 0.012$$

Deviation from SM

3.8σ
for the $R(D)$–$R(D^*)$ combination

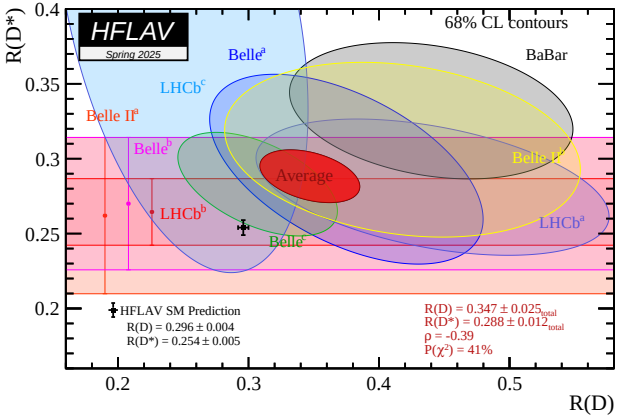

HFLAV average value (Spring 2025)

Kinematics of $B \to D^*(\to D\pi)\ell\nu_\ell$

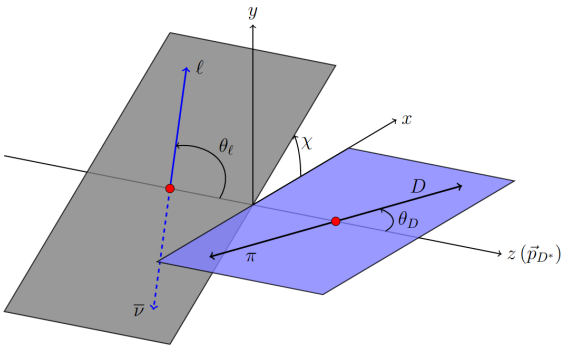

$\ell = \mu, e$. Picture is taken from arXiv:1907.02257

$$B \to D^* \ell \nu_\ell, \quad D^* \to D\pi, \quad D \to K\pi$$

- Hints of NP in $R(D^*)$ can be further studied and characterized through angular analyses
- Helicity angles: $\cos\theta_\ell$, $\cos\theta_D$, χ
- Momentum transfer squared: $q^2 = (p_{B^0} - p_{D^*})^2 = (p_\ell + p_\nu)^2$
- The decay $D^* \to D\pi$ depends on q^2 (form factors from Isgur-Wise function or lattice QCD)
- Otherwise $B \to D^*\ell\nu$ kinematics are fully described by the helicity angles

Angular Analysis

- Full angular differential decay rate for $\overline{B} \to D^*(\to D\pi)\ell\nu_\ell$ using $\cos\theta_\ell, \cos\theta_D, \chi$ (The QCD effects are absorbed in $J_i(q^2)$) :

$$\frac{d^4\hat{\Gamma}^{(\ell)}}{dq^2\, d\cos\theta_\ell\, d\cos\theta_D\, d\chi} = \frac{3}{8\pi}\sum_i^{12} J_i^{(\ell)}(q^2) f_i(\cos\theta_\ell, \cos\theta_D, \chi)$$

- Differential distributions can be expressed as one-dimensional projections. In this case, only 5 (4 in CP-averaged measurements) angular coefficients can be extracted.

$$\frac{1}{\hat{\Gamma}^{(\ell)}}\frac{d\hat{\Gamma}^{(\ell)}}{d\cos\theta_\ell} = \frac{1}{2} + \langle A_{FB}^{(\ell)}\rangle \cos\theta_\ell + \frac{1}{4}\left(1 - 3\langle \tilde{F}_L^{(\ell)}\rangle\right)\frac{3\cos^2\theta_\ell - 1}{2}$$

$$\frac{1}{\hat{\Gamma}^{(\ell)}}\frac{d\hat{\Gamma}^{(\ell)}}{d\cos\theta_D} = \frac{3}{4}(1 - \langle F_L^{(\ell)}\rangle)\sin^2\theta_D + \frac{3}{2}\langle F_L^{(\ell)}\rangle \cos^2\theta_D$$

$$\frac{1}{\hat{\Gamma}^{(\ell)}}\frac{d\hat{\Gamma}^{(\ell)}}{d\chi} = \frac{1}{2\pi} + \frac{2}{3\pi}\langle S_3^{(\ell)}\rangle \cos 2\chi + \frac{2}{3\pi}\langle S_9^{(\ell)}\rangle \sin 2\chi$$

D^{*-} longitudinal polarisation in $B^0 \to D^{*-}\tau^+\nu_\tau$

- "State of the art" analysis from LHCb
- In a simplified model only D^* longitudinal polarisation can be measured from $cos\theta_D$ distribution in $B^0 \to D^{*-}\tau^+\nu_\tau$ decays based on 2011,2012 + 2015,2016 statistics Phys. Rev. D **110**, 092007 (2024)

$q^2 < 7\,\mathrm{GeV}^2/c^4$: $0.51 \pm 0.07\,(\mathrm{stat}) \pm 0.03\,(\mathrm{syst})$

$q^2 > 7\,\mathrm{GeV}^2/c^4$: $0.35 \pm 0.08\,(\mathrm{stat}) \pm 0.02\,(\mathrm{syst})$

q^2integrated : $0.43 \pm 0.06\,(\mathrm{stat}) \pm 0.03\,(\mathrm{syst})$

- Results compatible with the Belle result and SM [Phys.Rev.D 98 (2018) 9, 095018, Eur.Phys.J.C 79 (2019) 3, 268]

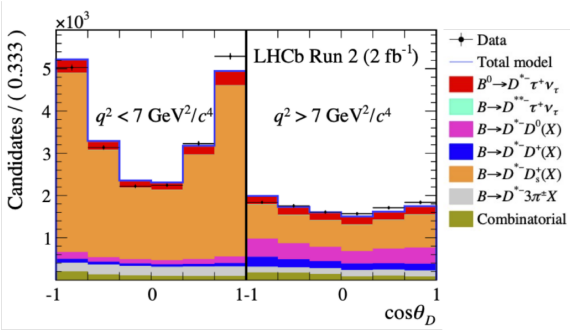

Angular observables and Wilson coefficients

- Full set of angular observables provides better sensitivity to NP effects

The dependence of angular observables on Wilson coefficients

Vector : $C_V^{\ell\ell'} = C_{V_R}^{\ell\ell'} + C_{V_L}^{\ell\ell'}$, Pseudovector : $C_A^{\ell\ell'} = C_{V_R}^{\ell\ell'} - C_{V_L}^{\ell\ell'}$, Pseudoscalar : $C_P^{\ell\ell'} = C_{S_R}^{\ell\ell'} - C_{S_L}^{\ell\ell'}$

Observable	$\lvert C_A\rvert^2$	$\lvert C_V\rvert^2$	$\lvert C_P\rvert^2$	$\lvert C_T\rvert^2$	$\mathrm{Re}(C_A C_V^*)$	$\mathrm{Re}(C_A C_P^*)$	$\mathrm{Re}(C_A C_T^*)$	$\mathrm{Re}(C_V C_P^*)$	$\mathrm{Re}(C_V C_T^*)$	$\mathrm{Re}(C_P C_T^*)$
$F_L^{D^*}$	O(1)	–	O(1)	O(1)	–	$O(m_\ell/\sqrt{q^2})$	$O(m_\ell/\sqrt{q^2})$	–	$O(m_\ell/\sqrt{q^2})$	O(1)
A_{FB}	(m^2)	–	–	(m^2)	✓	(m)	(m)	–	(m)	–
J_{1c}	O(1)	–	O(1)	O(1)	–	$O(m_\ell/\sqrt{q^2})$	$O(m_\ell/\sqrt{q^2})$	–	–	–
J_{1s}	O(1)	O(1)	–	O(1)	–	$O(m_\ell/\sqrt{q^2})$	$O(m_\ell/\sqrt{q^2})$	–	$O(m_\ell/\sqrt{q^2})$	–
J_{2c}	O(1)	–	–	O(1)	–	–	$O(m_\ell/\sqrt{q^2})$	–	–	–
J_{2s}	O(1)	–	–	O(1)	–	–	–	–	–	–
J_3	O(1)	O(1)	–	O(1)	–	–	–	–	–	–
...	...	...	...	...	...	...	...	...	...	...

The table is taken from Eur. Phys. J. C **81**, 984 (2021).

The q^2 dependence

- Different NP currents show distinct dependencies on q^2
- Ideally, the measured angular coefficients should be separated into q^2 bins (the q^2 bins used in the analysis are shown in the plot)

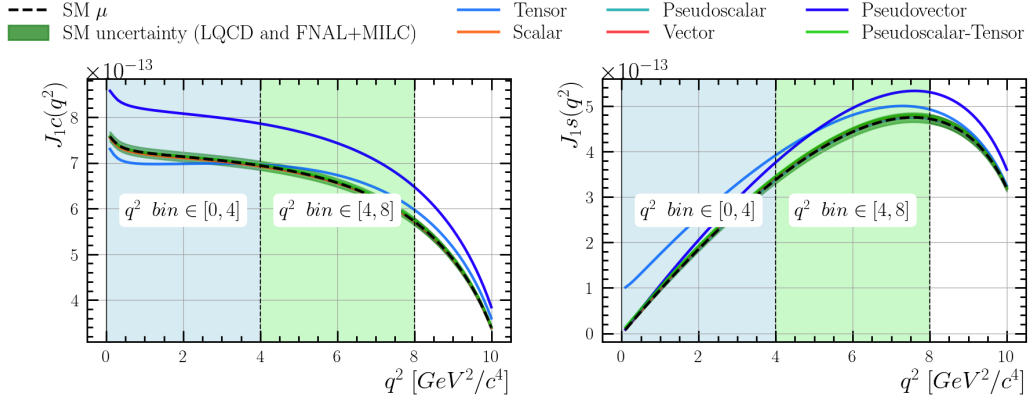

$J_{1c}(q^2)$ for SM μ and new physics scenarios, each with amplitude of 10% of SM. Plots generated with EOS package

Outline

The LHCb Experiment at the LHC

- LHCb is one of the experiments based at the Large Hadron Collider (LHC) at CERN, Geneva
- **High production rate:** Proton–proton collisions have a large $b\bar{b}$ production cross-section, yielding many B mesons.
- Initially designed to perform precision measurements in the beauty quark sector
- Physics program has been extended:
  - Charm physics
  - Hadron spectroscopy
  - Top quark physics
  - Heavy ions
  - Electro-weak and Higgs physics
  - ...

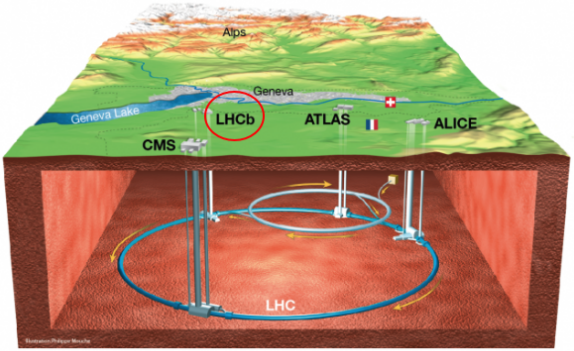

The LHCb detector at the LHC

LHCb Integrated Luminosity and Runs

Definition of data taking periods

- **Run 1:** 2010–2012
- **Run 2:** 2015–2018
- **Run 3:** 2022–present

Period	$\mathcal{L}$ (fb^{-1})
Run 2: 2015	0.30
Run 2: 2016	1.6
Run 2: 2017	1.7
Run 2: 2018	2.1

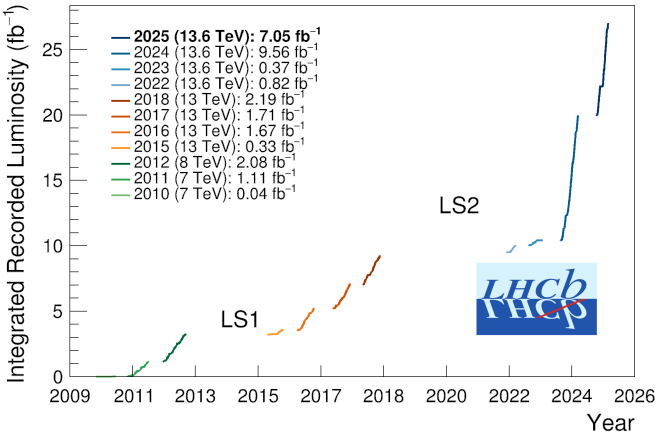

LHCb detector in Run 2

Single-arm forward spectrometer:

- Forward angular coverage, designed for the heavy flavour physics with ($\sim 25\%$ *of* $b\bar{b}$ *pairs in detector acceptance*)
- Efficient trigger, excellent performance of tracking and vertexing, powerful particle identification, allow to perform high precision heavy flavour physics study (e.g. measurement of B decays)

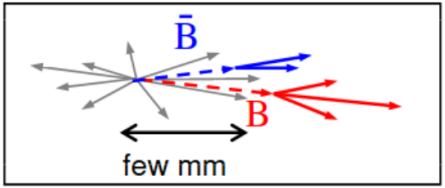

a few mm from the **PV (Primary Vertex), i.e. the proton-proton interaction point**, before decaying in the inner tracking detector (Vertex Locator).

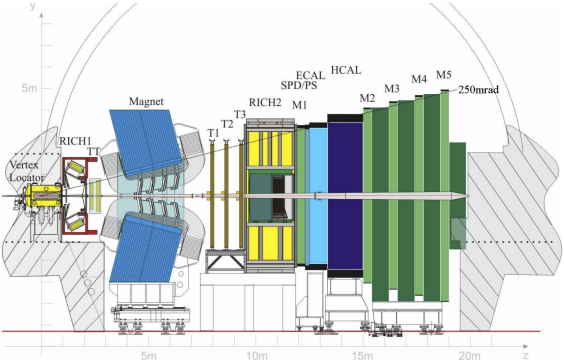

Outline

Analysis motivation

- **Hints of LFU violation:** There were hints of LFU violation in angular observables measurements of data from Belle detector [Eur. Phys. J. C 81 (2021) 984], [JHEP 11 (2019) 133] in $\langle A_{FB}^{\mu} \rangle - \langle A_{FB}^{e} \rangle$. The QCD uncertainties cancel out in difference

- Goal: Measure 12 angular coefficients per lepton flavour ($\ell = e, \mu$) for $B \to D^* e\nu_e$ and $B \to D^* \mu\nu_\mu$ in two q^2 bins: $[0, 4]\,\text{GeV}^2$ and $[4, 8]$ based on LHCb 2016-2018 Data. Cross-check Belle results on the hadron collider

- *Belle detector : e^+e^- collider experiment at the KEKB accelerator (Japan), operating at the $\Upsilon(4S)$ resonance to produce entangled $B\bar{B}$ meson pairs. It was designed as a high-luminosity B-factory for precision flavour physics.*

Methodology – Background templates

- Purely experimental variable (useful to suppress background, p_{B^0} is estimated differently than for the angles) :
  $M^2_{\text{miss}} = (p_{B^0} - p_{D^*} - p_\ell)^2$
- To fit the kinematic distribution of the decay in the presence of backgrounds, a template fit is performed
- The missing mass squared (M^2_{miss}) is a powerful kinematic variable to separate signal from background

Main background decays:

1. Semileptonic decays of $B^{0,+}$ to higher excited D^* states (a mixture of $D_0^*(2300)$, $D_1(2420)$, $D_1(2430)$, etc.), collectively denoted as D^{**}
2. $B^{0/+} \to D^{*-} D_s^+ \left(\to (\tau^+ \to \ell^+ \nu_{\ell\tau} \overline{\nu_\ell}) \nu_\tau\right) X$
3. Double-charm decays $B^{0/+} \to D^* D \left(\to \ell^+ \nu_\ell\right) X$
4. Lepton misidentification

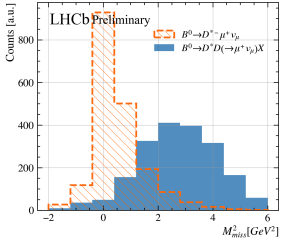

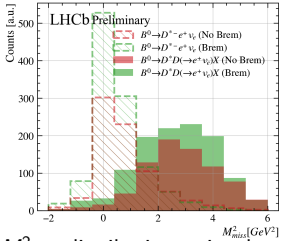

M^2_{miss} distributions: signal vs. $B^{0/+} \to D^* D \left(\to \ell^+ \nu_\ell\right) X$

Bremsstrahlung Correction

- Bremsstrahlung mainly from interaction with detector material (Coulomb field of atoms)
- Energy loss rises linearly with E/m^2 (mostly affecting electrons)
- If photon emitted **before the magnet**, momentum measurement is biased
- Most electrons emit a hard brem photon before the magnet
- Strategy: find the brem photon and add its energy back (Brem photon recovery efficiency $\sim 60\%$)
- Electrons categorised into:
  - **With brem photon**
  - **No brem photon**

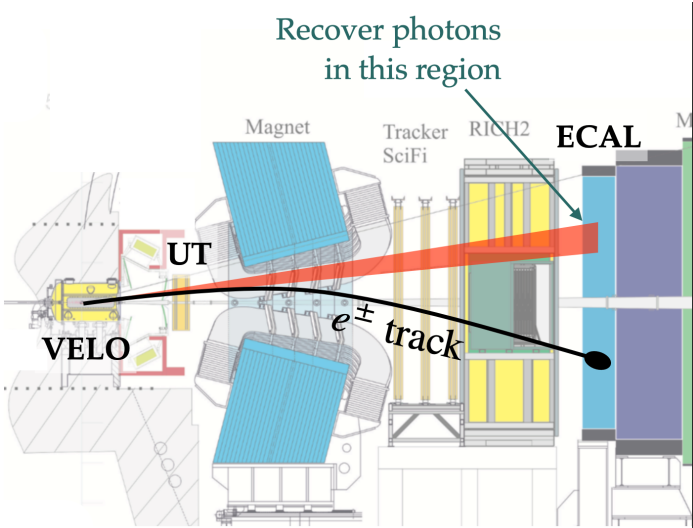

Methodology Overview: Angular Analysis of $B^0 \to D^{*-}\ell^+\nu_\ell$ Decays

Methodology

- **4D Template Fit:** helicity angles & M^2_{miss} using MC and data-driven templates
- **Binning Scheme:**

$$[\cos\theta_D, \cos\theta_\ell, \chi, M^2_{\text{miss}}, q^2] = [3, 3, 6, 5, 2]$$

- **Independent Fits:** performed separately for electron and muon channels
- **Electron Channel:** combined fit on two bremsstrahlung categories

Neutrino Reconstruction

Kinematic reconstruction of the ν from the visible decay products ($D^*\ell$, denoted as Y), using the decay topology, precise VELO vertexing, and the B mass

$$|\vec{p}_{B^0}| = \frac{(m_Y^2 + m_{B^0}^2)|\vec{p}_Y|\cos\theta_{B^0,Y} \pm E_Y\sqrt{(m_{B^0}^2 - m_Y^2)^2 - 4m_{B^0}^2|\vec{p}_Y|^2\sin^2\theta_{B^0,Y}}}{2(E_Y^2 - |\vec{p}_Y|^2\cos^2\theta_{B^0,Y})}$$

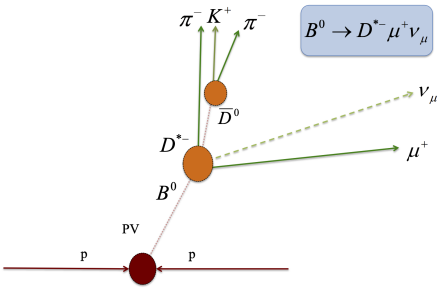

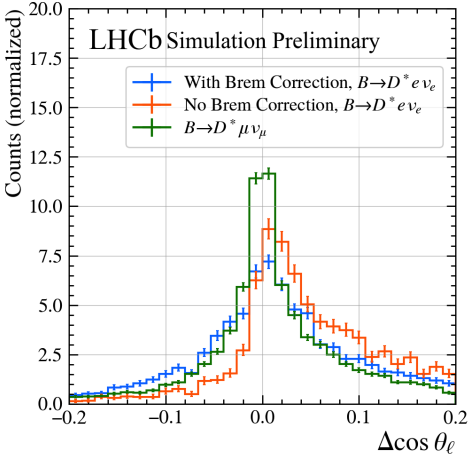

Reconstruction resolution: difference between true and reconstructed variables

Efficiency

- Efficiencies are parametrised as smooth 4D function of the kinematic variables.
- Events with $q^2 > 8$ GeV^2 are excluded due to low efficiency.

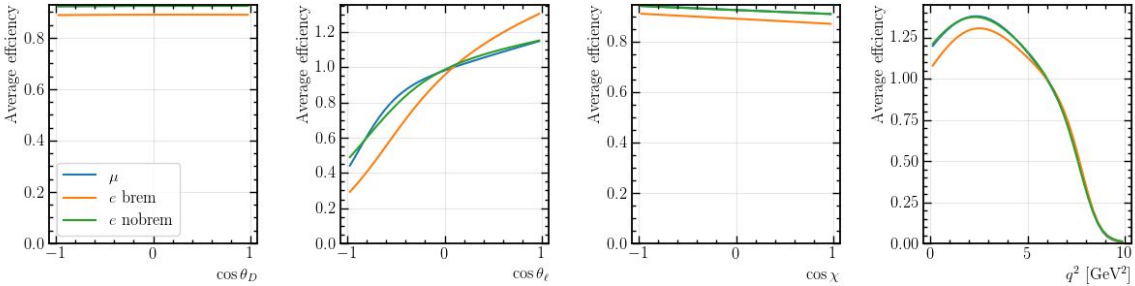

Resolution and Response Matrices

- Detector resolution and misreconstruction cause migration of events between bins.
- Migration can be modeled via a response matrix

$$R_{ij} = P(\text{reco bin } R_i \mid \text{true bin } T_j),$$

determined from MC.

- Resolution in q^2 is corrected by a response matrix.
- Resolution in angular space is taken into account by weights in templates

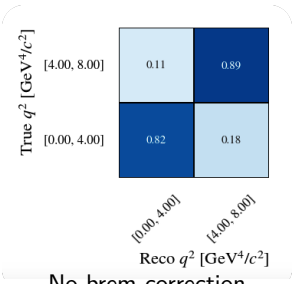

No brem correction

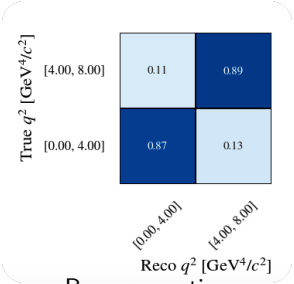

Brem correction

The response matrix and templates for $B^0 \to D^* e\nu_e$ is obtained separately for each bremsstrahlung category

Signal templates accounting for detector effects

- To take into account kinematic-dependent detector efficiencies and resolution a template fit approach is implemented JHEP11(2019)133.
- The decay density is a linear sum of 12 angular terms. Effects of background, efficiency, and resolution are also linear → 4D unbinned density = binned 4D templates
- The goal is to incorporate efficiency and resolution effects into binned angular terms — templates
- This can be achieved by using the true angular coefficients from the MC simulation

Unbinned angular functions

$$\frac{d^4\hat{\Gamma}^{(\ell)}}{dq^2 d\cos(\theta_\ell) d\cos(\theta_D) d\chi} = \frac{3}{8\pi} \sum_i^{12} J_i^{(\ell)}(q^2) \; f_i(\cos(\theta_\ell), \cos(\theta_D), \chi) =$$

Binned angular templates

$$\frac{3}{8\pi} \sum_i^{12} J_i^{(\ell)}(q^2) \; h_i(\cos(\theta_\ell), \cos(\theta_D), \chi)$$

Signal templates

After integrating over q^2, the PDF is expressed in terms of the angular coefficients $I_i = \frac{\int (J_i(q^2) + \bar{J}_i(q^2)) dq^2}{2}$:

$$
\begin{aligned}
p(\theta_D, \theta_\ell, \chi) = \frac{d^3\hat{\Gamma}^\ell}{d\cos\theta_D \, d\cos\theta_\ell \, d\chi} \propto\ & I_{1c} \cos^2\theta_D + I_{1s} \sin^2\theta_D \\
& + [\, I_{2c} \cos^2\theta_D + I_{2s} \sin^2\theta_D \,] \cos 2\theta_\ell \\
& + [\, I_{6c} \cos^2\theta_D + I_{6s} \sin^2\theta_D \,] \cos\theta_\ell \\
& + [\, I_3 \cos 2\chi + I_9 \sin 2\chi \,] \sin^2\theta_\ell \sin^2\theta_D \\
& + [\, I_4 \cos\chi + I_8 \sin\chi \,] \sin 2\theta_\ell \sin 2\theta_D \\
& + [\, I_5 \cos\chi + I_7 \sin\chi \,] \sin\theta_\ell \sin 2\theta_D \, .
\end{aligned}
$$

Full fit PDF

$$\text{PDF}(\theta_D, \theta_\ell, \chi) = \text{PDF}^{\text{noBrem}}(\theta_D, \theta_\ell, \chi) + \text{PDF}^{\text{Brem}}(\theta_D, \theta_\ell, \chi)$$

$$\text{PDF}^{(d)}(\theta_D, \theta_\ell, \chi) = \left[\tfrac{1}{3}\left(4 - 6\, I_{1s} + I_{2c} + 2\, I_{2s}\right) h_{I_{1c}} + \sum_i I_i\, h_{I_i} \right] f_{\text{sig}}^{(d)}$$
$$+ f_{D^* \text{ excited}}^{(d)}\, h_{D^* \text{ excited}} + f_{B_s^0 \to D_s^{**} e\nu}^{(d)}\, h_{B_s^0 \to D_s^{**} e\nu} + f_{D^* D_s(\to\tau)}^{(d)}\, h_{D^* D_s(\to\tau)}$$
$$+ f_{\text{Combinatorial}}^{(d)}\, h_{\text{Combinatorial}} + f_{\text{Double charm}}^{(d)}\, h_{\text{Double charm}}$$

Notes:

- Angular coefficients I_i are **shared** across fit categories d = noBrem, Brem (11 free parameters)
- Fractions $f^{(d)}$ are **independent** for each dataset (10 free parameters, 2 fixed parameters)
- Templates h_{I_i} are the fixed shapes (34 templates)
- **Blinding:** All fit parameters are **blinded** by applying a random shift, and the result is multiplied by a random number

Fit validation with bootstrapping, $B \to D^* e\nu_e$

- The SM signal + background MC fit sample is bootstrapped
- The validation checks are used to quantify potential biases and ensure the fit is robust
- Pull distributions between true and fitted angular coefficients for $B \to D^* e\nu_e$ are shown
- Iteration of 1000 template fits reproduces true angular coefficients reliably

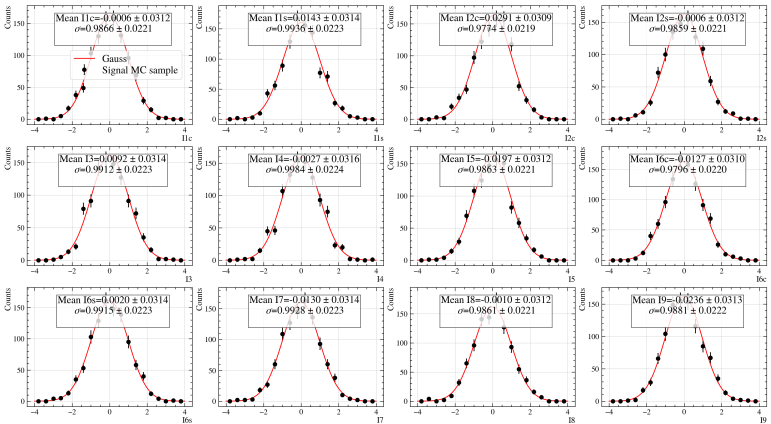

4D Data template fit results, projections, $B \to D^* e\nu_e$

- Binning scheme for data:
  $[\cos\theta_D, \cos\theta_\ell, \chi, M^2_{\text{miss}}] = [3,3,6,5]$
- Binning edges are chosen to have approximately equal statistics in each angular bin
- Missing mass bin edges are evenly spaced

Template fit of data 2016-2018. Fit projection:

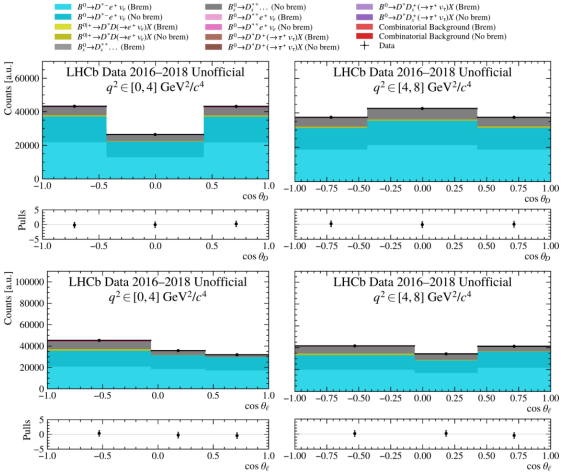

4D Data template fit results, projections, $B \to D^* e\nu_e$

Template fit of data 2016-2018. Fit projection:

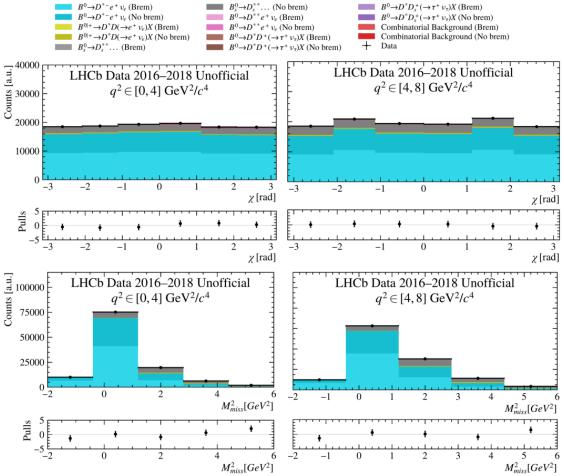

Blinded fit results, $B \to D^* e\nu_e$

Fit Parameter	$q^2 \in [0, 4]$ GeV$^2/c^4$	$q^2 \in [4, 8]$ GeV$^2/c^4$
l1c	0.8519 ± 0.0130 (stat.) ± 0.0091 (syst.)	0.5404 ± 0.0104 (stat.) ± 0.0083 (syst.)
l1s	1.1207 ± 0.0045 (stat.) ± 0.0057 (syst.)	1.3005 ± 0.0036 (stat.) ± 0.0102 (syst.)
l2c	-0.4659 ± 0.0218 (stat.) ± 0.0136 (syst.)	-0.3572 ± 0.0143 (stat.) ± 0.0122 (syst.)
l2s	0.9511 ± 0.0089 (stat.) ± 0.0087 (syst.)	0.9688 ± 0.0084 (stat.) ± 0.0229 (syst.)
l6c	0.5940 ± 0.0168 (stat.) ± 0.0141 (syst.)	0.7015 ± 0.0094 (stat.) ± 0.0146 (syst.)
l6s	0.8777 ± 0.0068 (stat.) ± 0.0107 (syst.)	1.0518 ± 0.0050 (stat.) ± 0.0134 (syst.)
l3	0.5545 ± 0.0073 (stat.) ± 0.0090 (syst.)	0.4315 ± 0.0065 (stat.) ± 0.0307 (syst.)
l4	0.3849 ± 0.0107 (stat.) ± 0.0058 (syst.)	0.4423 ± 0.0062 (stat.) ± 0.0223 (syst.)
l5	1.1225 ± 0.0074 (stat.) ± 0.0157 (syst.)	1.1085 ± 0.0054 (stat.) ± 0.0277 (syst.)
l7	0.8552 ± 0.0076 (stat.) ± 0.0163 (syst.)	0.8372 ± 0.0059 (stat.) ± 0.0105 (syst.)
l8	0.5043 ± 0.0106 (stat.) ± 0.0076 (syst.)	0.5070 ± 0.0069 (stat.) ± 0.0157 (syst.)
l9	0.9348 ± 0.0066 (stat.) ± 0.0070 (syst.)	0.9032 ± 0.0054 (stat.) ± 0.0227 (syst.)
Signal fraction no Brem	1.0250 ± 0.0046	1.0464 ± 0.0047
D^* excited states fraction no Brem	0.5522 ± 0.0089	0.5342 ± 0.0072
$B_s^0 \to D_s^{**} e^+ \nu_e$ fraction no Brem	0.9123 ± 0.0042	0.9311 ± 0.0043
$D^* Ds(\to \tau \ldots)$ fraction no Brem	0.6034 ± 0.0060	0.5933 ± 0.0051
Combinatorial fraction no Brem	0.5552 ± 0.0054	0.5398 ± 0.0033
Double charm fraction no Brem	0.1500 ± 0.0135	0.1507 ± 0.0113
Signal fraction with Brem	1.3737 ± 0.0041	1.3892 ± 0.0040
D^* excited states fraction with Brem	0.6850 ± 0.0045	0.6708 ± 0.0047
$B_s^0 \to D_s^{**} e^+ \nu_e$ fraction with Brem	0.1024 ± 0.0028	0.1390 ± 0.0038
Double charm fraction with Brem	0.3136 ± 0.0060	0.3125 ± 0.0062
χ^2/ndof	227/162	230/198

Main uncertainties breakdown for $B \to D^\star e\nu_e$

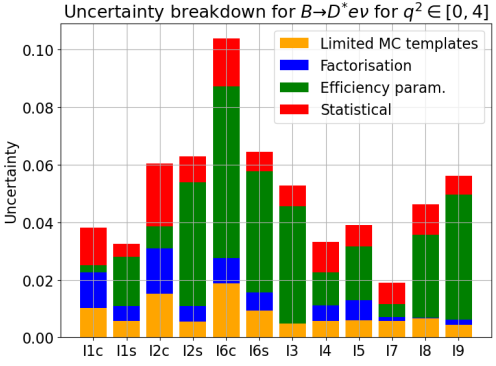

(a) $q^2 \in [0, 4]$ GeV$^2/c^4$

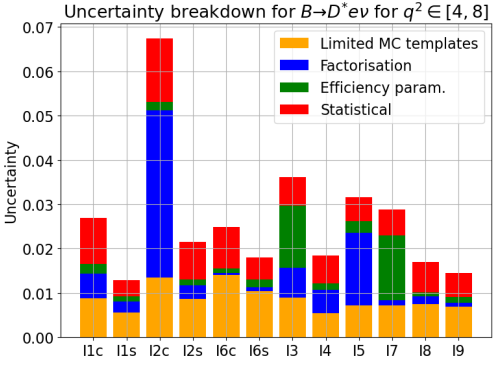

(b) $q^2 \in [4, 8]$ GeV$^2/c^4$

Main systematic uncertainties for the decay $B \to D^\star e\nu_e$ in two q^2 regions.

Analysis status and outlook

- Complementary test of LFU and probing full set of Wilson Coefficients in $B \to D^* \ell\nu_\ell$
- Template fit of $B \to D^* \mu\nu_\mu$ and $B \to D^* e\nu_e$ procedure allow to extract all 12 angular coefficients from the 4D fit
- $B \to D^* e\nu_e$ blinded coefficient were obtained with Brem information included in the templates
- Measurements of angular coefficients in $B^0 \to D^* \mu\nu_\mu$ and $B^0 \to D^* e\nu_e$ decays at LHCb are competitive with Belle, providing a factor ~ 7 improvement in statistical precision and a factor ~ 3 improvement in overall precision.
- Toy studies conducted in different q^2 regions:
  - Empty bins in the background templates do not influence the results of the fit
  - Systematic uncertainty of the limited MC statistic is evaluated
- Systematic for template fit from limited MC statistics, model dependence, q^2 acceptance, q^2 factorisation, efficiency parameterization are evaluated

Plans:

- Finalise systematics : estimate the model-dependant uncertainty for the main background cocktail - D**, the contribution and interference of non-resonant $B \to D\pi\mu\nu$ amplitude.
- Unblind the results

Outline

The LHCb Run 3 Upgrade

- Major upgrade to collect data with $\sim 5\times$ higher luminosity:

$$\mathcal{L} = 2 \times 10^{33}\,\mathrm{cm}^{-2}\mathrm{s}^{-1}$$

- Increasing pile-up: $\mu = 5.3$ (pp collisions per bunch crossing)
- Full replacement of tracking detectors to cope with higher occupancy
- New addition: **SMOG2** (System for Measuring Overlap with Gas) – injects small amounts of noble gas into the beam pipe and turns LHCb into a fixed-target experiment
- What about triggering?

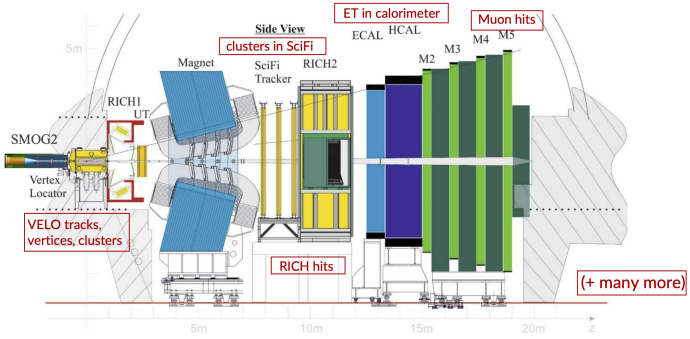

Reference: LHCb-TDR-12

LHCb Run 3 Trigger Upgrade

Motivation: Limitations of Run 2 trigger

- First-level hardware stage (L0) saturates trigger yields with increasing luminosity
- Tight momentum/energy requirements at L0 selections
- Run 3 solution: Replace the 1 MHz-limited hardware trigger L0 by a software-only trigger on GPUs
- Perform reconstruction at 30 MHz for High Level Trigger (HLT)

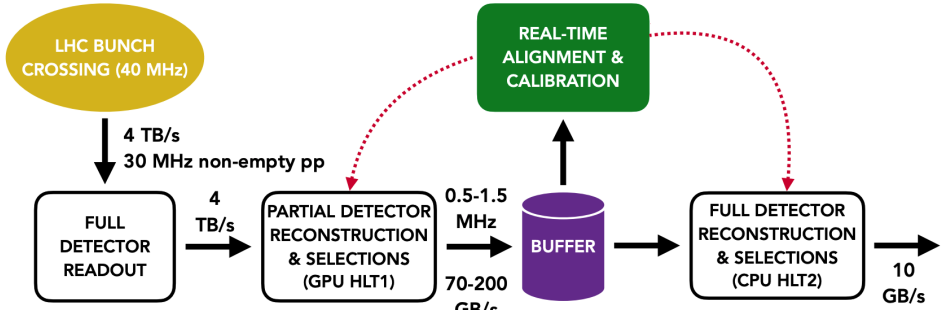

LHCb HLT1 PV reconstruction

- **PV precision:** Essential for neutrino momentum reconstruction, decay-time measurements, and background suppression

Developments for a parallel algorithm for primary vertex (PV) reconstruction running on HLT1 farm on GPUs. Currently, the default PV reconstruction algorithm is beam-dependent (new for Run 3):

1. Extrapolation of the VELO track states to the point of closest approach (POCA) to the beamline
2. Filling a histogram with a density distribution around z (POCA) of the extrapolated tracks
3. Searching for peaks in this histogram
4. Peaks are seeds used for iterative vertex fit

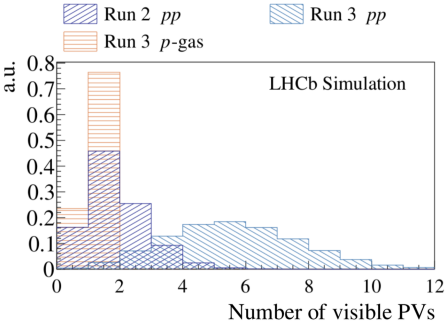

Higher visible pp and p-gas interactions compared to Run 2 require PV reconstruction optimisation.
Eur. Phys. J. C (2025) 85:609

PV reconstruction dependence on beamline position

- The study aimed to evaluate the impact of beam position on the reconstructed PV position
- MC simulations with 2024 data-taking conditions were used
- Thresholds on beamline position were identified beyond which PV reconstruction becomes inefficient
- When these thresholds are reached, the beamline position is recalibrated

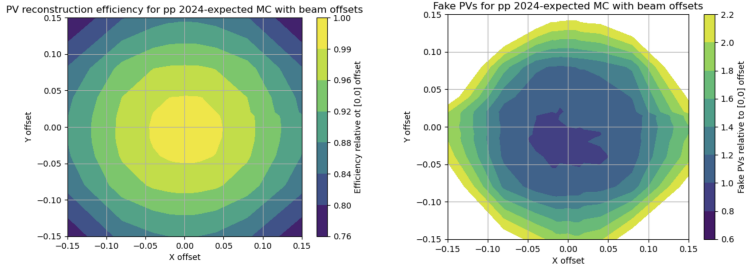

Target case to stay within 99.9% of efficiency $r = \sqrt{(x^2 + y^2)} = 0.02$

PV reconstruction dependence on beamline inclination

- Previously, beamline inclination was not considered in the PV reconstruction
- Noticeable effect was observed on the System for Measuring Overlap With Gas (SMOG), a fixed-target experiment employed as part of LHCb

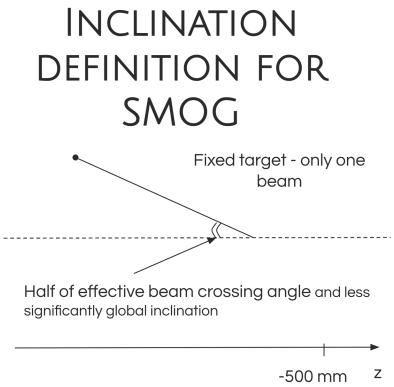

PV reconstruction dependence on beamline inclination

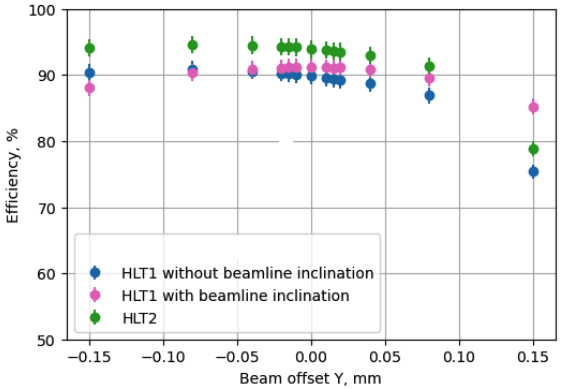

Comparison of HLT1 PV finders for SMOG2 region. Reconstruction efficiency with and without beamline inclination included in the fit, and HLT2 PV finder

Development Results

Main focus: Participation in detector commissioning during Run 3, primarily in PV reconstruction on HLT1

- Threshold for beamline position recalibration has been determined
- Beamline inclination incorporated into the default PV reconstruction procedure used in data taking
- Additionally, PV resolution monitor developed and operational.
  - Enables continuous monitoring of PV reconstruction performance
  - Results are processed in real time during Run 3 data taking

Outline

Future prospects

- Run 3: luminosity $2 \times 10^{33}\,\mathrm{cm}^{-2}\mathrm{s}^{-1}$ ($\sim 5\times$ Run 2), $\sim 23\,\mathrm{fb}^{-1}$ by mid-2026
- More data $\Rightarrow$ reduced statistical/ some systematic limits
- $R(D)$–$R(D^*)$ tension persists ($\sim 4\sigma$)
- Angular observables are very promising for resolving potential New Physics structure
- $b \to c\ell\nu_\ell$ angular analyses, next steps :
  - Full angular information in $B^0 \to D^{*-}\mu^+\nu_\mu$ and $B^0 \to D^{*-}e^+\nu_e$ (presented in this thesis)
  - Full angular analysis with $B^0 \to D^{*-}\tau^+\nu_\tau$
  - Measurements involving higher excited states of D^* and D_s

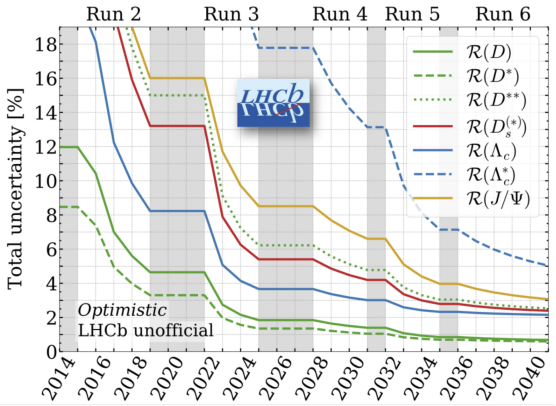

Data sample up to year

[Rev. Mod. Phys. 94, 015003 (2022)]

Future prospects: Excited D_s states

Reminder: Sensitivity of angular observables to Wilson coefficients

Obs.	$\lvert C_A\rvert^2$	$\lvert C_V\rvert^2$	$\lvert C_P\rvert^2$	$\lvert C_T\rvert^2$	$\Re(C_A C_V^*)$	$\Re(C_A C_P^*)$	$\Re(C_A C_T^*)$	$\Re(C_V C_P^*)$	$\Re(C_V C_T^*)$	$\Re(C_P C_T^*)$
...	...	...	...	...	...	...	...	...	...	...

Sensitivity limited for some NP couplings (e.g. scalar C_S). Pseudovector final states ($J^P = 1^+$) give complementary info.

- Interest in $D_{s1}(2460)$, $D_{s1}(2536)$:
  - NP searches in the SL decays with pseudovector D_{s1}: $B_s^0 \to D_{s1}(2536)^+ \mu^- \nu_\mu$ (couplings different from $D^* \ell \nu$)
  - Near $D^* K$ threshold ($T_{c\bar{s}}(2900)$ near $D^* K^*$) -> possible molecular admixture
- Involved in Run 2 amplitude analyses testing the resonance vs. molecular nature: $D_{s1}^+(2460, 2536) \to D_s^+ \pi^+ \pi^-$
- The preliminary analysis reveals that the observed decay patterns cannot be explained by a $\pi^+\pi^-$ scalar and tensor components
- **Future prospects:** Hadronic spectroscopy, Measurements of $R(D_{s1})$ and angular analyses

Conclusion and Plans

- **Analysis:**
  - Developed 4D template fit including efficiency, resolution, and backgrounds
  - Extracted all 12 angular coefficients for $B \to D^* e \nu_e$ and $B \to D^* \mu \nu_\mu$
  - Performed validation with toy studies and systematic evaluation
  - Results:
    - First blinded LHCb measurement of angular observables in $B \to D^* \ell \nu$
    - Competitive precision with Belle, complementary sensitivity to LFU tests
    - Plan : Finalise systematics for angular analysis and unblinding
- **LHCb trigger development**: Involvement in HLT1 commissioning during Run 3
- **Outlook:**
  - Future analyses on Run 3 with precision improvements
  - Many prospects on $b \to c \ell \nu$ angular analysis with D excited states

Thank you for your attention!

Backup Slides

Backup Slides

4D Data template fit results, projections, $B \to D^* \mu \nu_\mu$

- Binning scheme for data is $[\cos\theta_D, \cos\theta_\ell, \chi, M^2_{miss}] = [3,3,6,5]$
- Binning edges are placed to have approximately the same statistic in each bin for angles
- Missing mass bin edges are evenly spaced

Template fit of data 2016-2018. Fit projection:

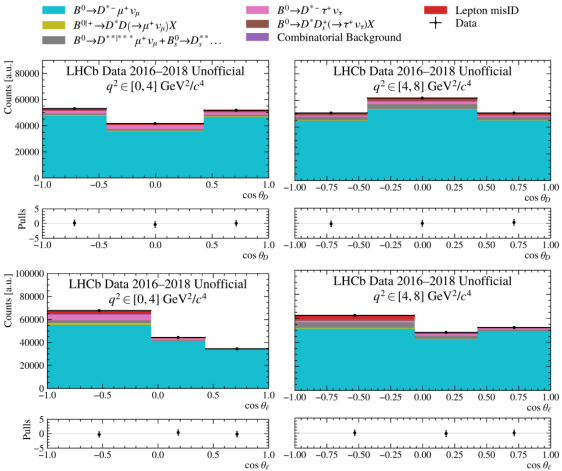

4D Data template fit results, projections, $B \to D^* \mu \nu_\mu$

Template fit of data 2016-2018. Fit projection:

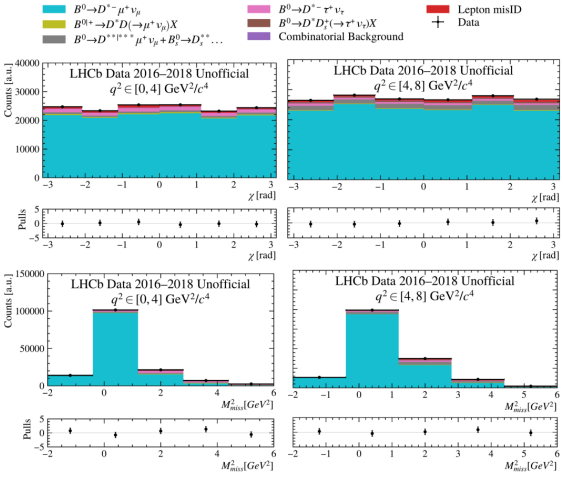

Blinded fit results, $B^0 \to D^* \mu \nu_\mu$

Fit Parameter	$q^2 \in [0, 4]$ GeV$^2/c^4$	$q^2 \in [4, 8]$ GeV$^2/c^4$
l_{1c}	1.0734 $\pm$ 0.0097 (stat.) $\pm$ 0.0118 (syst.)	0.8111 $\pm$ 0.0085 (stat.) $\pm$ 0.0068 (syst.)
l_{1s}	1.0901 $\pm$ 0.0032 (stat.) $\pm$ 0.0063 (syst.)	1.2656 $\pm$ 0.0030 (stat.) $\pm$ 0.0043 (syst.)
l_{2c}	0.2972 $\pm$ 0.0168 (stat.) $\pm$ 0.0176 (syst.)	0.4874 $\pm$ 0.0120 (stat.) $\pm$ 0.0123 (syst.)
l_{2s}	0.9539 $\pm$ 0.0067 (stat.) $\pm$ 0.0073 (syst.)	0.9918 $\pm$ 0.0069 (stat.) $\pm$ 0.0075 (syst.)
l_{6c}	0.3970 $\pm$ 0.0124 (stat.) $\pm$ 0.0179 (syst.)	0.4708 $\pm$ 0.0079 (stat.) $\pm$ 0.0101 (syst.)
l_{6s}	0.6336 $\pm$ 0.0050 (stat.) $\pm$ 0.0098 (syst.)	0.8024 $\pm$ 0.0043 (stat.) $\pm$ 0.0088 (syst.)
l_3	0.5116 $\pm$ 0.0059 (stat.) $\pm$ 0.0052 (syst.)	0.3996 $\pm$ 0.0055 (stat.) $\pm$ 0.0084 (syst.)
l_4	1.1110 $\pm$ 0.0084 (stat.) $\pm$ 0.0063 (syst.)	1.1771 $\pm$ 0.0051 (stat.) $\pm$ 0.0053 (syst.)
l_5	0.7793 $\pm$ 0.0065 (stat.) $\pm$ 0.0064 (syst.)	0.7926 $\pm$ 0.0045 (stat.) $\pm$ 0.0061 (syst.)
l_7	0.7684 $\pm$ 0.0064 (stat.) $\pm$ 0.0066 (syst.)	0.7699 $\pm$ 0.0050 (stat.) $\pm$ 0.0057 (syst.)
l_8	0.4618 $\pm$ 0.0083 (stat.) $\pm$ 0.0081 (syst.)	0.4541 $\pm$ 0.0057 (stat.) $\pm$ 0.0061 (syst.)
l_9	0.3016 $\pm$ 0.0058 (stat.) $\pm$ 0.0044 (syst.)	0.2781 $\pm$ 0.0045 (stat.) $\pm$ 0.0059 (syst.)
Signal fraction	1.5040 $\pm$ 0.0040	1.4959 $\pm$ 0.0029
Double charm fraction	0.0142 $\pm$ 0.0023	0.0063 $\pm$ 0.0019
D^* excited states fraction	0.5494 $\pm$ 0.0063	0.5836 $\pm$ 0.0061
$B_s^0 \to D_s^{**} \mu^+ \nu_\mu$ fraction	0.6379 $\pm$ 0.0028	0.6327 $\pm$ 0.0030
$D^* \tau$ fraction	0.7036 $\pm$ 0.0027	0.6820 $\pm$ 0.0037
$D^* Ds(\to \tau \ldots)$ fraction	0.9062 $\pm$ 0.0040	0.9179 $\pm$ 0.0047
Combinatorial fraction	0.8954 $\pm$ 0.0016	0.8921 $\pm$ 0.0012
Fake mu fraction	0.5062 $\pm$ 0.0097	0.5063 $\pm$ 0.0098
χ^2/ndof	204/162	217/198

Main uncertainties breakdown for $B \to D^{\star}\mu\nu_{\mu}$

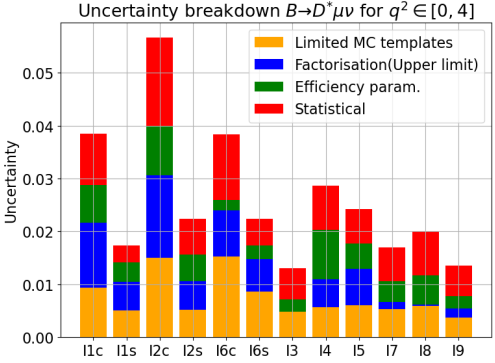

(a) $q^2 \in [0, 4]$ GeV$^2/c^4$

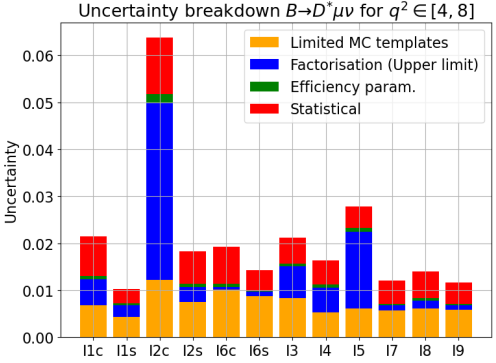

(b) $q^2 \in [4, 8]$ GeV$^2/c^4$

Main systematic uncertainties for the decay $B \to D^{\star}\mu\nu_{\mu}$ in two q^2 regions.

Comparison of Reweighting and Unfolding: Limited MC statistics

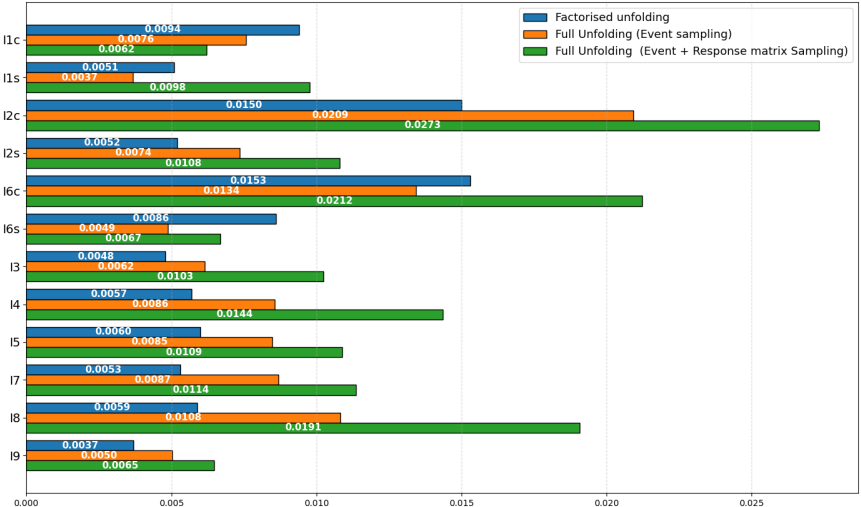

$B \to D^* e \nu_e$ in $q^2 \in [0, 4]$ GeV$^2/c^4$

Limited MC systematic uncertainty.

Resolution : Unfolding

- Detector resolution and misreconstruction cause migration of events between bins.
- To compare measured and theoretical distributions, we can apply resolution unfolding.
- Migration is modeled via a response matrix $R_{ij} = P(\text{reco bin } R_i \mid \text{true bin } T_j)$, determined from simulation for each decay mode.
- Unfolding with D'Agostini Bayes Iterative Method doi:10.1016/0168-9002(95)00274-X (RooUnfold package)

$$P(R_i \mid T_j) \approx \frac{N_{i,j}}{\sum_j N_{i,j}} \quad , \quad P(T_i|R_j) = \frac{P(R_j|T_i)P(T_i)}{\sum_l^{n_T} P(R_j|T_l)P(T_l)} \quad , \quad \hat{N}_i^T = \sum_j P(T_i|R_j)N_j^R$$

Iterate:

1. Start with prior from training truth $P^{(0)}(C_i)$
2. Compute $P^{(k)}(C_i|E_j)$
3. Estimate $\hat{N}_i^{T,(k)}$
4. Update priors and repeat

Motivation : Current experimental situation Belle II [Phys. Rev. Lett. 133, 131801 (2024)]

- Angular coefficients in $B \to D^*$ transitions determine form factors, enabling extraction of $|V_{cb}|$ (with LQCD input) and testing for BSM effects/LFU
- Key kinematic variable: $w = \frac{m_B^2 + m_{D^*}^2 - q^2}{2 m_B m_{D^*}}$

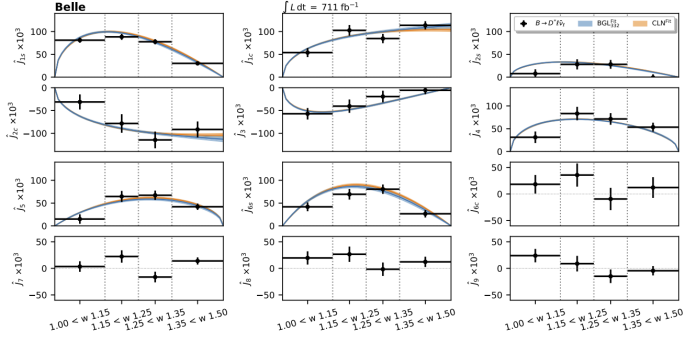

Resolution : Response matrices projections

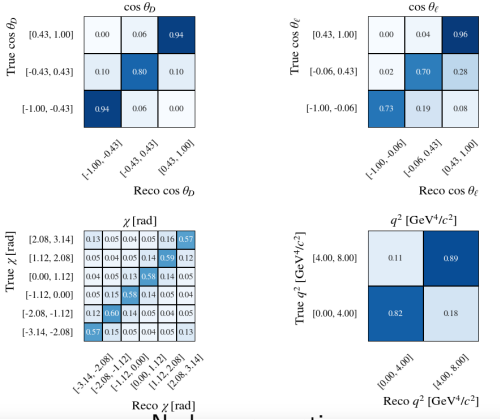

No brem correction

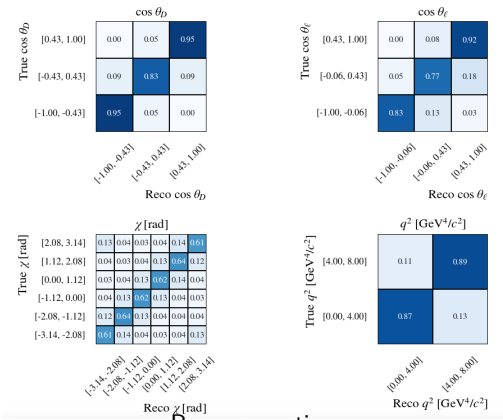

Brem correction

Projections of 9D response matrix for $B^0 \to D^* e \nu_e$. It is obtained separately for each brem category. The projection on M^2_{miss} is equal to identity matrix.

Orthogonal basis

Another advantage is the possibility to obtain angular coefficients directly from orthogonality, without the fit. The example with spherical harmonics:

$$\int Y_{lm}(\theta,\phi)\ Y_{l'm'}(\theta,\phi)\ \sin\theta\ d\theta\ d\phi = \delta_{ll'}\ \delta_{mm'} \tag{1}$$

$$\begin{aligned} p(\theta_D,\theta_\ell,\chi) = \frac{d^3\Gamma}{d\cos\theta_D\ d\cos\theta_\ell\ d\chi} \propto & I_{1c}\cos^2\theta_D + I_{1s}\sin^2\theta_D \\ & + [I_{2c}\cos^2\theta_D + I_{2s}\sin^2\theta_D]\cos 2\theta_\ell \\ & + [I_{6c}\cos^2\theta_D + I_{6s}\sin^2\theta_D]\cos\theta_\ell \\ & + [I_3\cos 2\chi + I_9\sin 2\chi]\sin^2\theta_\ell\sin^2\theta_D \\ & + [I_4\cos\chi + I_8\sin\chi]\sin 2\theta_\ell\sin 2\theta_D \\ & + [I_5\cos\chi + I_7\sin\chi]\sin\theta_\ell\sin 2\theta_D \end{aligned} \tag{2}$$

$$H_{l,m,n} = \int p(\theta_D,\theta_\ell,\chi)\ e_{l,m,n}(\theta_D,\theta_\ell,\chi)\ \sin\theta_D\ d\theta_D\ \sin\theta_\ell\ d\theta_\ell\ d\chi. \tag{3}$$

Combined Fit Results for $D_{s1}^{+} \to D_s^{+}\pi^{+}\pi^{-}$

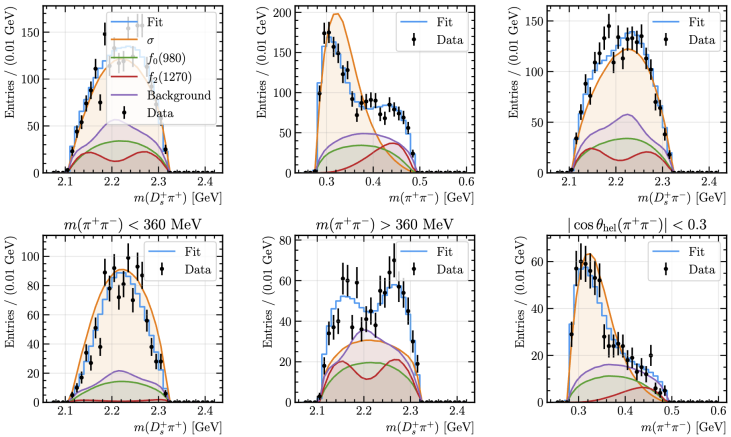

Combined fit with simplified model that include resonances only in $\pi\pi$ channel to $D_{s1}(2460)^{+}$ and $D_{s1}(2536)^{+}$ samples with resonances only in the $\pi^{+}\pi^{-}$ channel. This model includes three resonant contributions in the $\pi^{+}\pi^{-}$ channel: the σ, $f_2(1270)$ states, as well as the tail of the $f_0(980)$. Plots show Dalitz projections

Fit Results for $D_{s1}(2460)^+$ and $D_{s1}(2536)^+$

Table: Results of the fit to $D_{s1}(2460)^+$ and $D_{s1}(2536)^+ \to D_s^+\pi^+\pi^-$ data samples, including statistical uncertainties. The fit uses a model with σ and $f_2(1270)$ resonances with fixed Relativistic Breit–Wigner tails from $f_0(980)$.

Parameter	Combined Fit	$D_{s1}(2460)^+$ Only	$D_{s1}(2536)^+$ Only
$m(\sigma)$ (GeV)	$(346^{+8}_{-6}) \times 10^{-3}$	$(311.6^{+1.8}_{-1.7}) \times 10^{-3}$	$0.463^{+0.060}_{-0.031}$
$\Gamma(\sigma)$ (GeV)	$0.215^{+0.040}_{-0.030}$	$(66^{+7}_{-6}) \times 10^{-3}$	$0.38^{+0.13}_{-0.07}$
$\mathrm{Re}[a(f_2)]_{2460}$	-320 ± 70	$(-0.70^{+0.12}_{-0.11}) \times 10^3$	–
$\mathrm{Im}[a(f_2)]_{2460}$	30^{+50}_{-60}	$(-0.89^{+0.17}_{-0.18}) \times 10^3$	–
$\mathrm{Re}[a(f_2)]_{2536}$	280 ± 60	–	-28^{+28}_{-24}
$\mathrm{Im}[a(f_2)]_{2536}$	-80 ± 40	–	-37^{+20}_{-34}
$F_{2460}(\sigma)$ (%)	83.9	68.4	–
$F_{2460}(f_2(1270))$ (%)	16.2	31.6	–
$F_{2536}(\sigma)$ (%)	65.8	–	95.7
$F_{2536}(f_2(1270))$ (%)	34.2	–	4.3
$(\chi^2/N_{\mathrm{bins}})_{2460}$	146.5/60	81.5/60	–
$(\chi^2/N_{\mathrm{bins}})_{2536}$	114.5/60	–	67.5/60
$-\ln L$	-356.5	-349.9	-73.9

First orbital excitations of D_s mesons

First orbital excitations ($\ell = 1$): $\vec{j} = \vec{\ell} + \vec{s}_s$

Two states with s-quark $j = 1/2$, suppressed in $b \to c\ell\nu$ transition. Produced mostly in double charm decays ($b \to cW$, $W \to c\bar{s}$) :

$$D^*_{s0}(2317)^+ \ (J^P = 0^+), \quad D_{s1}(2460)^+ \ (J^P = 1^+)$$

Two states with $j = 3/2$, mostly produced in $b \to c\ell\nu$, $b \to c\pi$.:

$$D_{s1}(2536)^+ \ (J^P = 1^+), \quad D^*_{s2}(2573)^+ \ (J^P = 2^+)$$

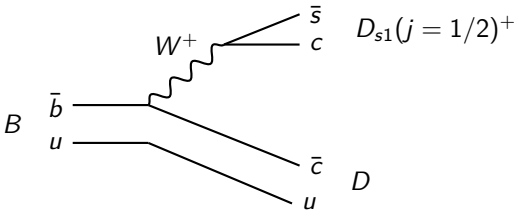

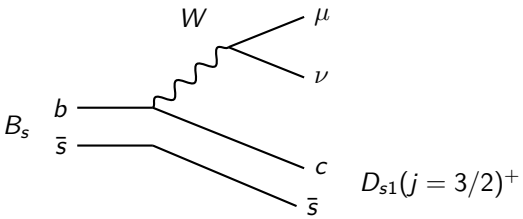

Dalitz plot studies of $D_{s1}^{+} \to D_s^{+}\pi^{+}\pi^{-}$

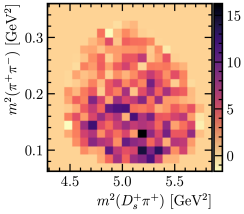

$D_{s1}(2536)^+$ Dalitz plot

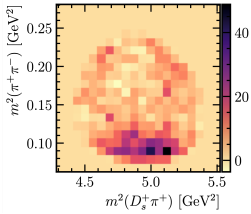

$D_{s1}(2460)^+$ Dalitz plot

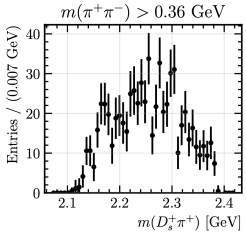

$D_{s1}(2536)^+$ projection slice on $m(D_s^+\pi^+)$

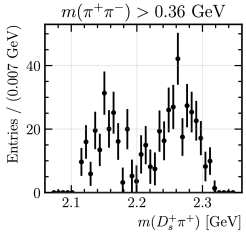

$D_{s1}(2460)^+$ projection slice on $m(D_s^+\pi^+)$

- Dalitz distributions reveal non-trivial dynamics.
- For $D_{s1}(2460)^+$ decays, the $\pi^+\pi^-$ spectrum shows:
  - a two-peak structure at higher mass.
- In contrast, the $D_{s1}(2536)^+$ distribution is relatively uniform.

Predictions for $\langle A_{\rm FB}^{(e)} \rangle$ vs. $\langle F_L^{(e)} \rangle$

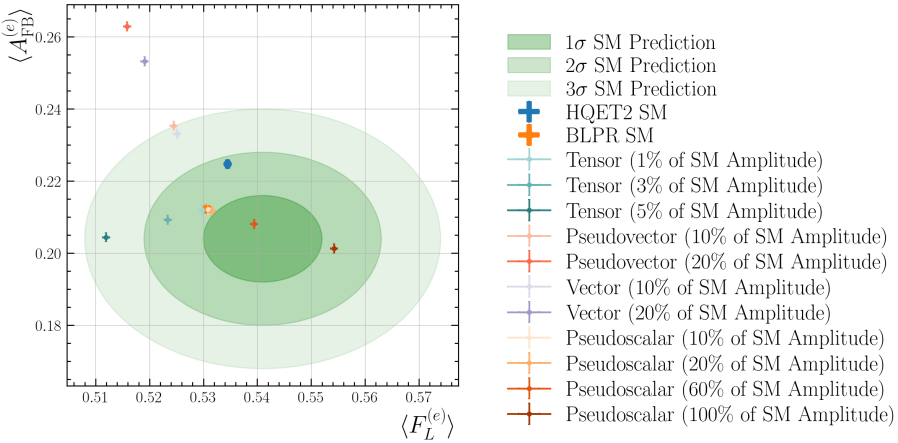

Model dependence bias of angular coefficients

Angular Coefficient	Tensor (10%)	Tensor (3%)	Pseudovector (10%)	Vector (10%)	Scalar (60%)	Pseudoscalar (60%)
I_{1c}	0.0379	0.0191	0.0002	0.0002	0.0044	0.0021
I_{1s}	0.0165	0.0016	0.0002	0.0001	0.0002	0.0003
I_{2c}	0.1680	0.0508	0.0015	0.0002	0.0121	0.0049
I_{2s}	0.0225	0.0081	0.0000	0.0001	0.0011	0.0016
I_3	0.0916	0.0136	0.0006	0.0002	0.0031	0.0032
I_4	0.0623	0.0160	0.0002	0.0001	0.0008	0.0033
I_5	0.0790	0.0232	0.0006	0.0004	0.0017	0.0009
I_{6c}	0.0465	0.0202	0.0001	0.0006	0.0060	0.0064
I_{6s}	0.0009	0.0003	0.0008	0.0008	0.0010	0.0011
I_7	0.1199	0.0420	0.0008	0.0000	0.0078	0.0080
I_8	0.1162	0.0406	0.0003	0.0011	0.0091	0.0093
I_9	0.1044	0.0230	0.0002	0.0001	0.0035	0.0033

Excited charm states

Table: Excited charm states and their decay modes modeled in this analysis. The masses and widths are taken from the PDG averages.

State	Mass (MeV)	Width (MeV)	Decay Modes
$D_0^*(2300)^{0,\pm}$	2343 ± 10	229 ± 16	$D^{*+}\pi^-, D^{*+}\pi^0\pi^0$
$D_1(2420)^{0,\pm}$	2422.1 ± 0.8	31.3 ± 1.9	$D^{*+}\pi^-$
$D_1(2430)^{0,\pm}$	2412 ± 9	314 ± 29	$D^{*+}\pi^-$
$D_2^*(2460)^{0,\pm}$	2461.1 ± 0.7	47.3 ± 0.8	$D^{*+}\pi^-, D^{*+}\pi^0$
$D_1^*(2600)^{0,\pm}$	2627 ± 10	141 ± 23	$D^{*+}\pi^-$
$D^*(2640)^{0,\pm}$	2412 ± 9	< 15	$D^{*+}\pi^-$
$D_3^*(2750)^{0,\pm}$	2763.1 ± 3.2	66 ± 5	$D^{*+}\pi^-$
$D(3000)^{0,\pm}$	2978.1 ± 8.7	188.1 ± 44.8	$D^{*+}\pi^-$
$D_{s1}(2536)^+$	2535.21 ± 0.28	0.92 ± 0.05	$D^{*+}K_S^0$
$D_{s2}(2573)^+$	2569.1 ± 0.8	16.9 ± 0.7	$D^{*+}K_S^0$

NP template fit $\cos\theta_\ell$, $B \to D^* \mu \nu_\mu$

- Example of sensitivity to NP of angular observable - $\langle A_{FB}^{\mu} \rangle$ for vector contribution with right helicity of b quark *V_qRIL* with different amplitudes (relative to the SM):

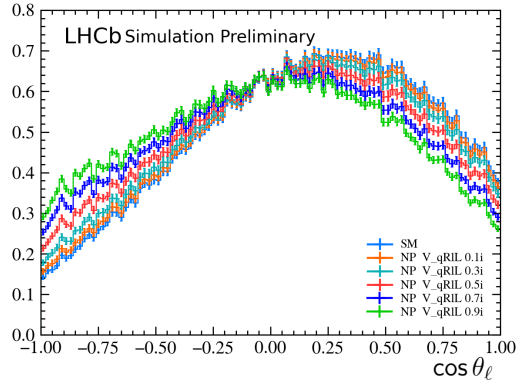

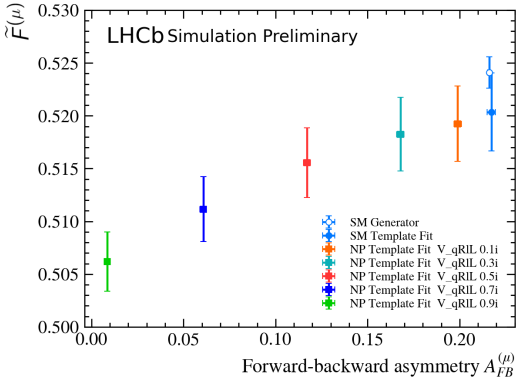

True MC distributions $B \to D^* \mu \nu_\mu$, $\cos\theta_D, \cos\theta_\ell, \chi$

- The unbinned fit on generator-level angles is performed to determine the true angular coefficients

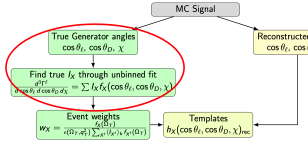

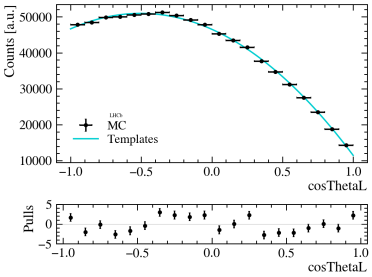

(a) $\cos\theta_\ell$

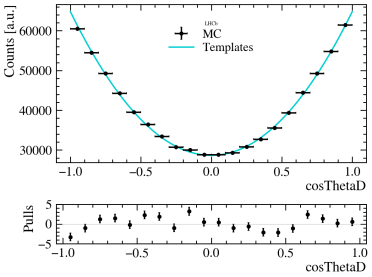

(b) $\cos\theta_D$

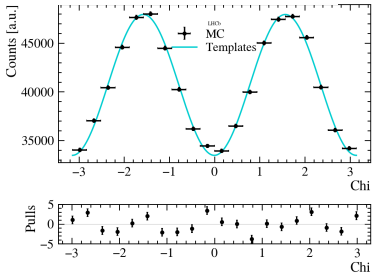

(c) χ

3D Unbinned fit projections of true MC sample

Methodology - $B \to D^* \ell \nu_\ell$

The following effects have a significant impact on the kinematic distributions and must be accounted for in the signal templates:

- Kinematic-dependent detector efficiencies
- Neutrino reconstruction procedure: approximation using the velocity of the reconstructed charm-lepton system, μH_c along the beam axis z: $\frac{(p_B)_z}{m_B} = \frac{(p_{\mu H_c})_z}{m_{\mu H_c}}$

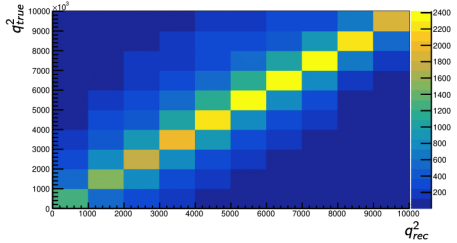

2D histogram of reconstructed q^2_{rec} versus true q^2_{true} distribution

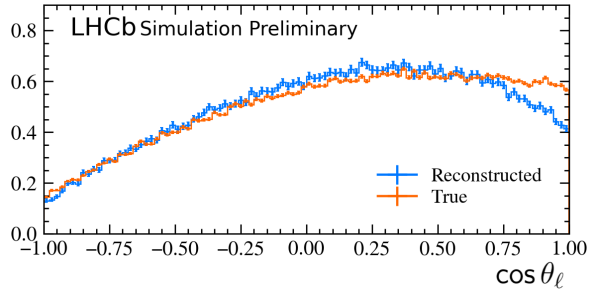

Methodology - Background templates

To suppress background contributions a template fit can be performed:

Background decays

1. $B^0 \to D^{**}\ell^+\nu_\ell$
2. $B^0 \to D^{***}\ell^+\nu_\ell$
3. $B^0 \to D^* D \left(\to \ell^+\nu_\ell\right) X$
4. $B^0 \to D^{*-} \left(\tau^+ \to \ell^+\nu_\tau\overline{\nu_e}\right)\nu_\tau$
5. $B^0 \to D^* D_s^+ \left(\to \left(\ell^+ \to \ell^+\nu_\tau\overline{\nu_e}\right)\nu_\tau\right) X$
6. $B^+ \to D^{**}\ell^+\nu_\ell$
7. $B^+ \to D^{***}\ell^+\nu_\ell$
8. $B^+ \to D^* D \left(\to \ell^+\nu_\ell\right) X$
9. $B^+ \to D^* D_s^+ \left(\to \left(\tau^+ \to \ell^+\nu_\ell\overline{\nu_\ell}\right)\nu_\tau\right) X$
10. $B_s^0 \to D_s^{**}\ell^+\nu_\ell$

Three variables of interest can efficiently separate signal from background:

- Lepton energy in B^0 frame (10 bins)
  $E_\ell^{B^0} \in [100,2500]$ MeV^2 —
  cannot be used due to correlation with $\cos\theta_\ell$
- Momentum transfer (2 bins) $q^2 = (p_{B^0} - p_{D^*})^2$
  $\in [0,4,8.5]$ GeV^2 —
  cannot be used due to q^2 bin splitting
- Squared missing mass (5 bins)
  $M^2_{miss} = (p_{B^0} - p_{D^*} - p_\ell)^2 \in$ [-2,6] GeV^2
- For each background 4D templates are created in variables $cos\theta_\ell, cos\theta_D$, χ and M^2_{miss}

NP template fit $\cos\theta_\ell$, $B \to D^* e \nu_e$

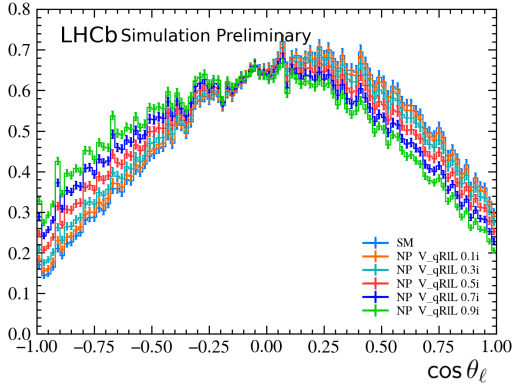

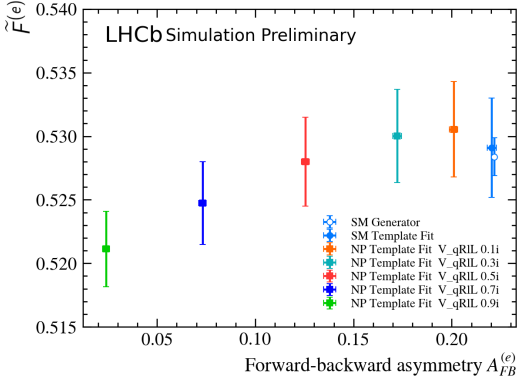

SMEFT vs WET

Energy scale

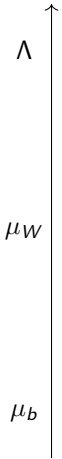

Theory

$$\mathcal{L}_{\text{full}} = ?$$

$\downarrow$ Integrating out unknown fields

$$\mathcal{L}_{\text{SMEFT}} = \mathcal{L}^{(4)}_{\text{SM}} + \frac{1}{\Lambda}\sum_k \tilde{C}^{(5)}_k Q^{(5)}_k + \frac{1}{\Lambda^2}\sum_k \tilde{C}^{(6)}_k Q^{(6)}_k + \mathcal{O}\left(\tfrac{1}{\Lambda^3}\right)$$

$\downarrow$ Integrating out heavy SM fields W,Z,h,t

$$\mathcal{L}_{\text{WET}} = \mathcal{L}_{\text{QED+QCD}} + \sum_k C^{(6)}_k O^{(6)}_k$$

BGL Parametrization

Model-independent parametrization [Boyd/Grinstein/Lebed]

1. Consider analytic structure $\rightarrow$ poles and cuts explicit
2. Remaining FFs $\rightarrow$ Taylor-expand in z
3. Apply QCD symmetries: unitarity, crossing
4. Calculate partonic part perturbatively

Result:

$$F(t) = \frac{1}{P(t)\,\phi(t)} \sum_{n=0}^{\infty} a_n \left[z(t, t_0)\right]^n$$

- a_n: real coefficients (unknowns)
- $P(t)$: Blaschke factors (poles below t_+)
- $\phi(t)$: outer function, ensures $\sum a_n^2 \leq 1$
- Series in z with bounded coefficients $|a_n| \leq 1$

HQET Parametrization

Heavy-Quark Expansion (HQET)

- Exploits heavy quark limit: $m_{b,c} \to \infty \to$ all $B \to D^{(*)}$ FFs given by **1 Isgur-Wise function**
- Systematic expansion in $1/m_{b,c}$ and α_s

CLN parametrization [Caprini+'97]

- HQET to order $1/m_{b,c}, \alpha_s$ plus perturbative corrections using QCD sum rules

Updated approach [Bernlochner/Ligeti/Papucci/Robinson'17]

- Identical HQET, includes higher-order corrections, updated correlations

Problems:

- Contradicts Lattice QCD (B $\to$ D and B $\to$ D*)
- Varying calculable parameters (e.g. $h_{A1}(1)$) $\to$ no longer systematic
- Residual uncertainty $\sim 5\%$, insufficient

Improved treatment:

- Include corelations betwen FF $1/m_c^2$
- BLPR model for $1/m_c^2 \to$ fewer parameters

Background templates : $D^{\star}D_s$

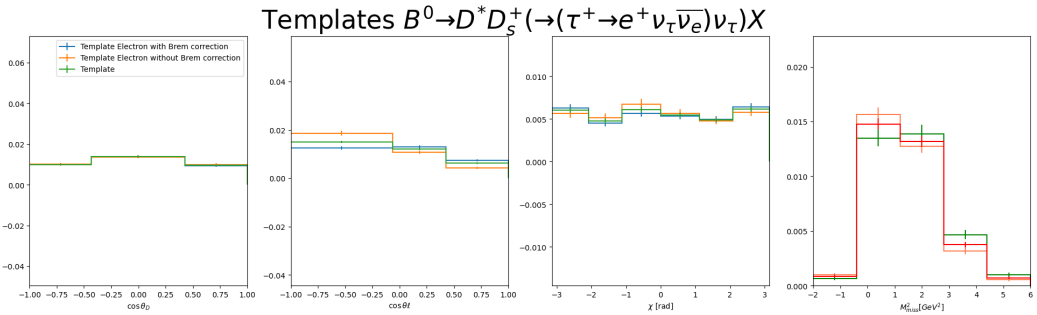

Background templates : $D**$ cocktail

Templates $B^0 \to D^{**} e^+ \nu_e$

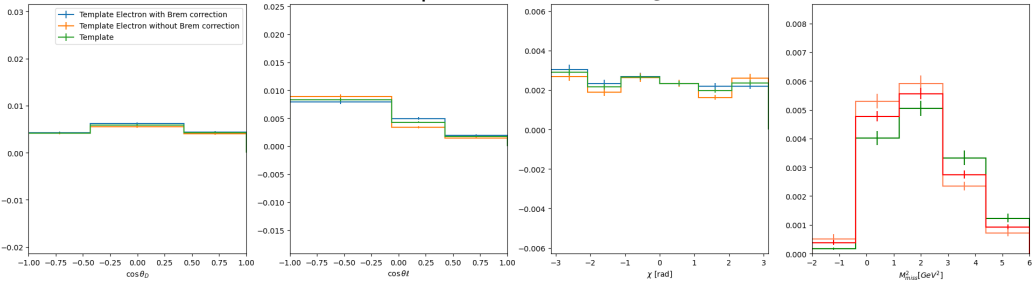

Toy studies. Bootstrapping of signal and background. Fractions

- Fractions of signal and background are also reliably retrieved from the template fit

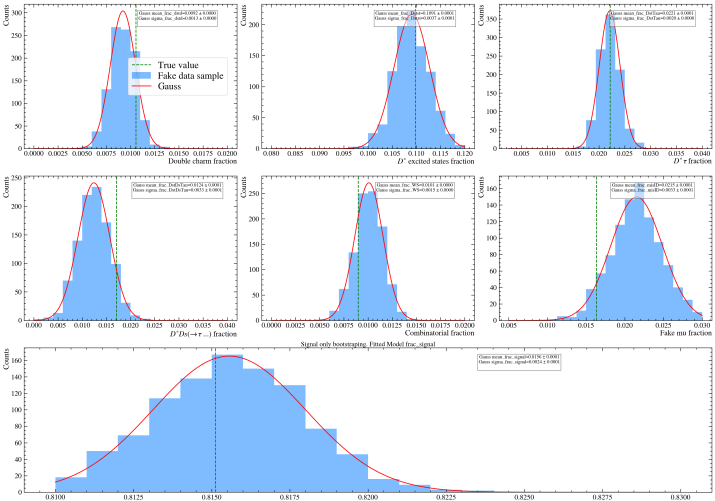

Methodology - Model independent template fit procedure

- To resolve these discrepancies between reconstructed and true angles the angular fit procedure described in JHEP 11, (2019) 133 can be used

$$\frac{1}{\hat{\Gamma}^{(\ell)}}\frac{d\hat{\Gamma}^{(\ell)}}{d\cos\theta_\ell} = \frac{1}{2}\cdot \boxed{1} + \langle A_{FB}^{(\ell)}\rangle \boxed{\cos\theta_\ell} + \frac{1}{4}(1-3\langle \tilde{F}_L^{(\ell)}\rangle)\frac{3\boxed{\cos^2\theta_\ell}-1}{2}$$

$$\frac{1}{\hat{\Gamma}^{(\ell)}}\frac{d\hat{\Gamma}^{(\ell)}}{d\cos\theta_D} = \frac{3}{4}(1-\langle F_L^{(\ell)}\rangle)\boxed{sin^2\theta_D} + \frac{3}{2}\langle F_L^{(\ell)}\rangle \boxed{\cos^2\theta_D}$$

$$\frac{1}{\hat{\Gamma}^{(\ell)}}\frac{d\hat{\Gamma}^{(\ell)}}{d\chi} = \frac{1}{2\pi}\cdot \boxed{1} + \frac{2}{3\pi}\langle S_3^{(\ell)}\rangle \boxed{\cos 2\chi} + \frac{2}{3\pi}\langle S_9^{(\ell)}\rangle \boxed{sin2\chi}$$

$$\frac{1}{\hat{\Gamma}^{(\ell)}}\frac{d\hat{\Gamma}^{(\ell)}}{d\cos\theta_\ell} = (\frac{1}{2}-\frac{1}{8}(1-3)\langle \tilde{F}_L^{(\ell)}\rangle)\boxed{h_{const,\theta_\ell}} + \langle A_{FB}^{(\ell)}\rangle \boxed{h_{\cos\theta_\ell}} + \frac{3}{8}(1-3\langle \tilde{F}_L^{(\ell)}\rangle)\boxed{h_{\cos^2\theta_\ell}}$$

$$\frac{1}{\hat{\Gamma}^{(\ell)}}\frac{d\hat{\Gamma}^{(\ell)}}{d\cos\theta_D} = \frac{3}{4}((1-\langle F_L^{(\ell)}\rangle)\boxed{h_{const,\theta_D}} + (3\langle F_L^{(\ell)}\rangle - 1)\boxed{h_{\cos^2\theta_D}}$$

$$\frac{1}{\hat{\Gamma}^{(\ell)}}\frac{d\hat{\Gamma}^{(\ell)}}{d\chi} = (\frac{1}{2\pi}-\frac{2}{3\pi}\langle S_3^{(\ell)}\rangle)\boxed{h_{const,\chi}} + \frac{2}{3\pi}\langle S_3^{(\ell)}\rangle \boxed{h_{(1+\cos 2\chi)}}$$

QDR : Muon

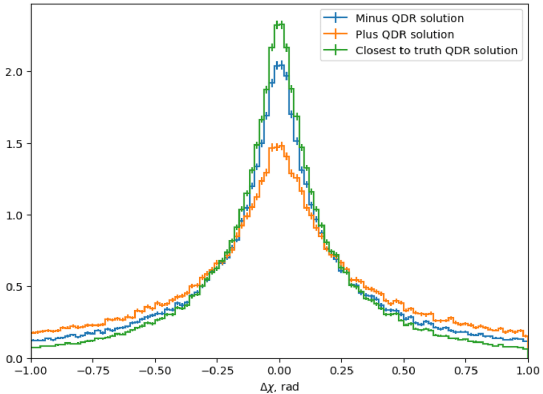

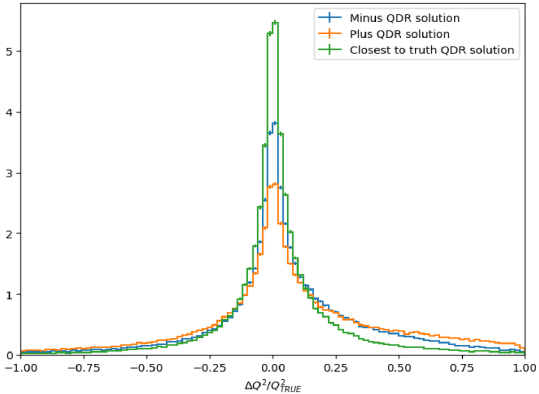

Reconstruction resolution for two solutions of QDR method in $B \to D^* \mu \nu_\mu$

True MC distributions $B \to D^* \mu \nu_\mu$, $\cos\theta_D, \cos\theta_\ell, \chi$

Generator SM:

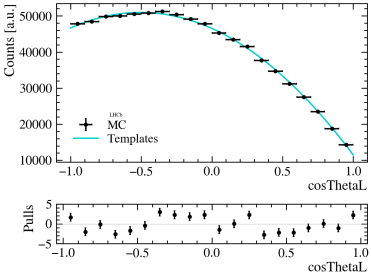

(a) $\cos\theta_\ell$

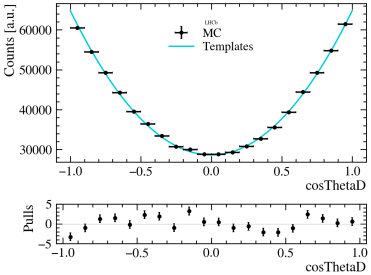

(b) $\cos\theta_D$

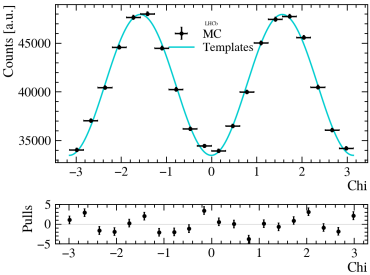

(c) χ

Fit of True MC distributions

4D Signal templates with Reconstruction and Resolution Effects

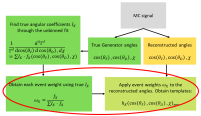

$\cos\theta_D^2 \cdot (2.0 \cdot \cos\theta_\ell^2 - 1.0)$ Template

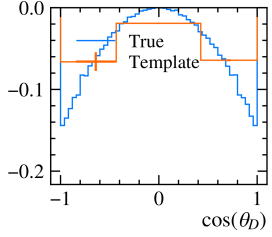

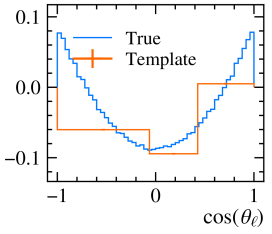

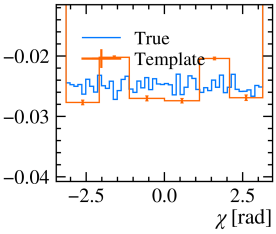

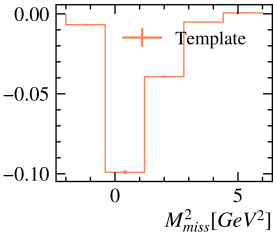

Projections for 4D template of reconstructed quantities of one out of 12 angular terms. The same templates are produced for each angular function. Binning scheme is $[\cos\theta_D, \cos\theta_\ell, \chi, M^2_{miss}] = [3,3,6,5]$. Angles binning edges are placed to have approximately the same statistic in each bin. Missing mass bin edges are evenly spaced

Results on MC - 1D fit

- Expected statistical uncertainty is estimated using the same selection criteria as in the ongoing analysis for $R(D^*)_{e/\mu}$, which is currently in the advanced state
- All of the results obtained on the simulation

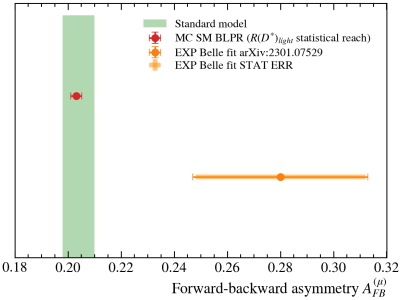

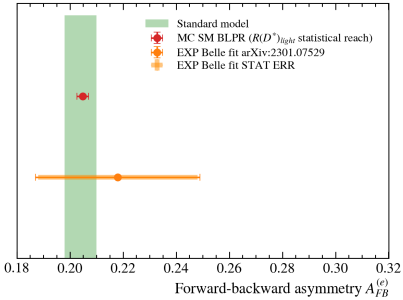

- Even though we had enough statistics in MC for 1D fit, the results were dominated by systematic uncertainties from a limited MC sample
- In total 300 Million events requested and processed for $B \to D^* e \nu_e$ and $B \to D^* \mu \nu_\mu$

Processing pipelines

- Control mode for MC correction: $B^+ \to J/\psi(\to \ell^+\ell^-)K^{*+}$
- Charged isolation tool → machine-learning algorithm, scan every track and compare against $D^{*+}\mu^-/D^{*+}e^-$ vertex

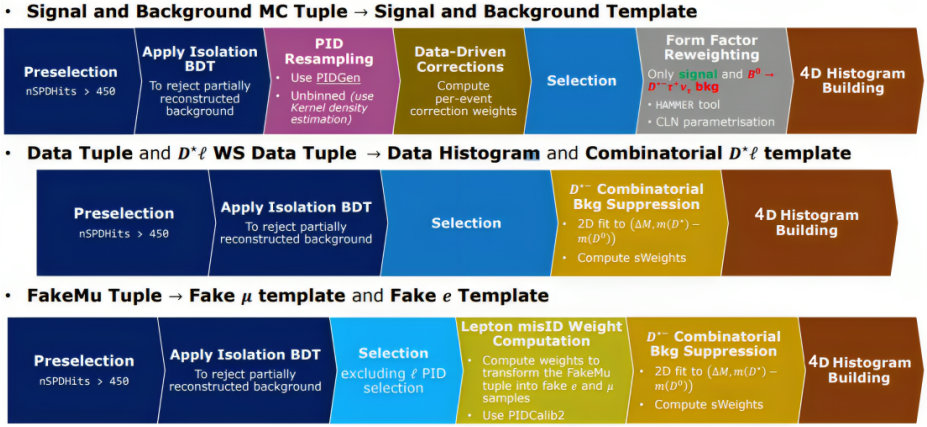

Toy studies. Toy study to assess empty bin effect.Q2 splitting. Angular coefficients

- Momentum transfer (5 bins) $q^2 = (p_{B^0} - p_{D^*})^2 \in [0,10]$ GeV^2
- To test the effect of limited statistics, a toy study was done on the last bin of q^2 from 7.5 to 10 GeV^2

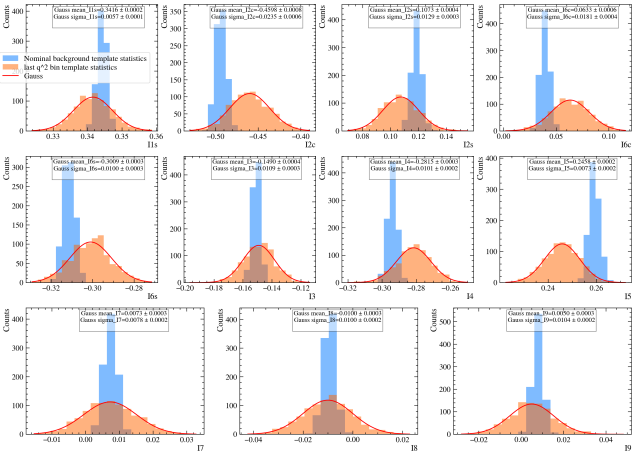

Data 2D projection. Restricted phase space region

- The study was done to check if we have empty bins in the templates and what binning we should use
- Both in Data and MC there is a phase space restricted region on 2D distribution of M^2_{miss} and $cos(\theta_\ell)$
- This region was excluded from the fit

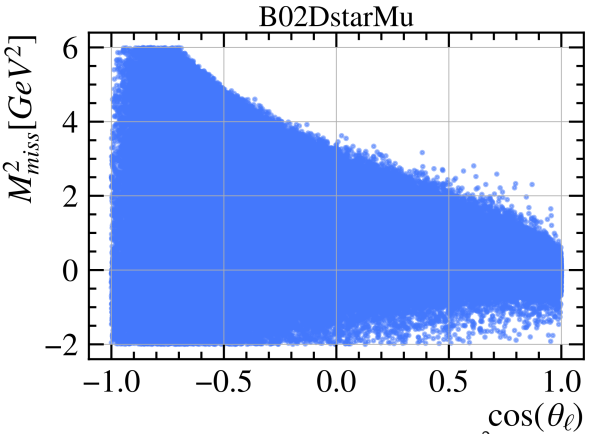

Data for 2016-2018 combined. Scattering plot of M^2_{miss} and $cos(\theta_\ell)$ distributions)

Toy studies. Bootstrapping of signal and background. Q2 splitting. Angular coefficients

- Momentum transfer (5 bins) $q^2 = (p_{B^0} - p_{D^*})^2 \in [0,10]$ GeV^2
- To test the effect of limited statistics, a toy study was done on the last bin of q^2 from 7.5 to 10 GeV^2

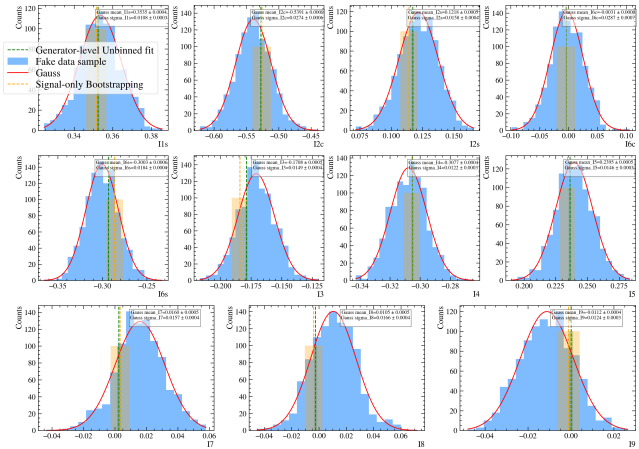

Toy studies. Bootstrapping of signal and background. Q2 splitting. Fractions

- The decrease in statistics results in a wider distribution. Nonetheless, this does not introduce a systematic bias into the measurement

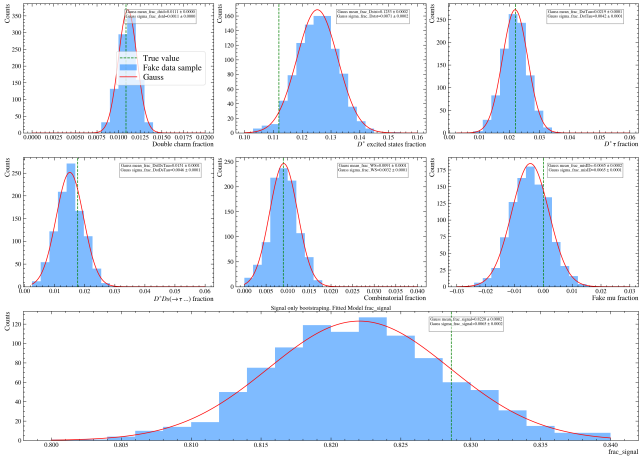

Background Templates

- Expected number of events for each background was estimated using branching ratios from PDG, trigger, stripping, and selection efficiencies
- Background modes MC simulation was requested, processed and combined with already existed samples
- Have enough statistics in the templates now to separate main background modes
- $B_s^0 \to D_s^{**}\ell^+\nu_\ell$, $B^0 \to D^{**|***}\ell^+\nu_\ell$, and $B^+ \to D^{**|***}\ell^+\nu_\ell$ distributions are similar, they were combined, relative ratio is constrained
- Double charm $B^0 \to D^* D$ and $B^+ \to D^* D$ are combined as well

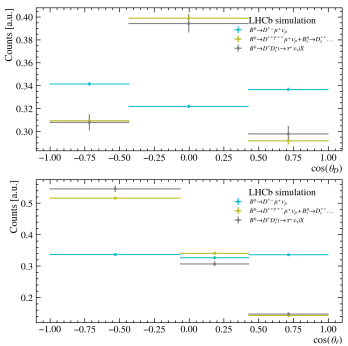

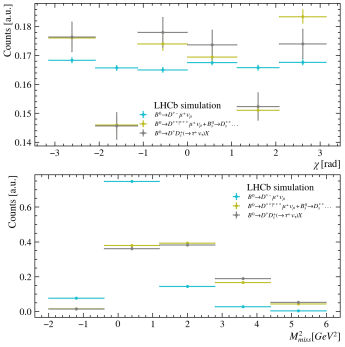

Toy studies on Full MC. Q2 splitting. Correlation matrix

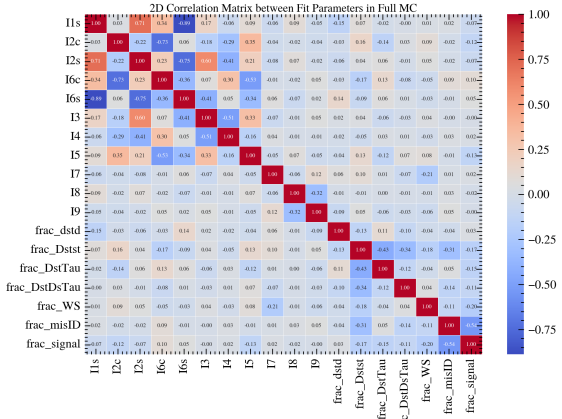

Resolve correlations

- One possible way to resolve high correlation is to transition to an orthogonal angular function
- Might be useful for the calculation of Forward-backward asymmetry or D^* polarisation

$$
\begin{aligned}
e_0 &= \frac{\sqrt{2}}{4\sqrt{\pi}} \\
e_1 &= \frac{\sqrt{10}\cdot\left(3\sin^2\theta - 2\right)}{8\sqrt{\pi}} \\
e_2 &= \frac{\sqrt{30}\cos^2\theta\cos\theta_L}{4\sqrt{\pi}} \\
e_3 &= \frac{\sqrt{6}\cdot\left(5\sin^2\theta - 2\right)\cos\theta_L}{8\sqrt{\pi}} \\
e_4 &= \frac{5\sqrt{2}\cdot\cos^2\theta\left(3\cos^2\theta_L - 1\right)}{8\sqrt{\pi}} \\
e_5 &= \frac{\sqrt{10}\left(-15\sin^2\theta\sin^2\theta_L + 10\sin^2\theta + 6\sin^2\theta_L - 4\right)}{16\sqrt{\pi}}
\end{aligned}
\tag{4}
$$

$$
\begin{aligned}
e_6 &= \frac{15\sin^2\theta\sin^2\theta_L\cos 2\chi}{16\sqrt{\pi}} \\
e_7 &= \frac{15\sin^2\theta\sin^2\theta_L\sin 2\chi}{16\sqrt{\pi}} \\
e_8 &= \frac{15\sin 2\theta\sin 2\theta_L\cos\chi}{16\sqrt{\pi}} \\
e_9 &= \frac{15\sin 2\theta\sin 2\theta_L\sin\chi}{16\sqrt{\pi}} \\
e_{10} &= \frac{3\sqrt{5}\sin 2\theta\sin\theta_L\cos\chi}{8\sqrt{\pi}} \\
e_{11} &= \frac{3\sqrt{5}\sin 2\theta\sin\theta_L\sin\chi}{8\sqrt{\pi}}
\end{aligned}
\tag{5}
$$

Methodology - Background templates

To suppress background contributions a template fit can be performed:

Background decays

1. $B^0 \to D^{**}\ell^+\nu_\ell$
2. $B^0 \to D^{***}\ell^+\nu_\ell$
3. $B^0 \to D^* D \left(\to \ell^+\nu_\ell\right) X$
4. $B^0 \to D^{*-} \left(\tau^+ \to \ell^+\nu_\tau\overline{\nu_e}\right)\nu_\tau$
5. $B^0 \to D^* D_s^+ \left(\to \left(\ell^+ \to \ell^+\nu_\tau\overline{\nu_e}\right)\nu_\tau\right) X$
6. $B^+ \to D^{**}\ell^+\nu_\ell$
7. $B^+ \to D^{***}\ell^+\nu_\ell$
8. $B^+ \to D^* D \left(\to \ell^+\nu_\ell\right) X$
9. $B^+ \to D^* D_s^+ \left(\to \left(\tau^+ \to \ell^+\nu_\ell\overline{\nu_\ell}\right)\nu_\tau\right) X$
10. $B_s^0 \to D_s^{**}\ell^+\nu_\ell$

Three variables of interest can efficiently separate signal from background:

- Lepton energy in B^0 frame (10 bins)
  $E_\ell^{B^0} \in [100,2500]$ MeV^2 —
  cannot be used due to correlation with $\cos\theta_\ell$
- Momentum transfer (2 bins) $q^2 = (p_{B^0} - p_{D^*})^2$
  $\in [0,4,8.5]$ GeV^2 —
  cannot be used due to q^2 bin splitting
- Squared missing mass (5 bins)
  $M^2_{miss} = (p_{B^0} - p_{D^*} - p_\ell)^2 \in$ [-2,6] GeV^2
- For each background 4D templates are created in variables $cos\theta_\ell, cos\theta_D$, χ and M^2_{miss}

Template Fit Formalism

Goal: Incorporate efficiency ϵ and resolution (bin migration) into decay rate template approximation.

1. Starting point:

$$\frac{d^2\Gamma}{dq_T^2\, d\Omega_T} \propto \sum_X J_X(q_T^2)\, f_X(\Omega_T)$$

Integrated over q_T^2:

$$\frac{d\Gamma}{d\Omega_T} \propto \sum_X \left[\int J_X(q_T^2)\, dq_T^2\right] f_X(\Omega_T)$$

2. In reconstructed variables (subscript R), include detector effects:

$$\frac{d\Gamma}{d\Omega_R} \propto \sum_X \left[\int J_X(q_T^2)\, f_X(\Omega_T)\, \epsilon(\Omega_T, q_T^2)\, M(\Omega_T, q_T^2\ |\Omega_R, q_R^2)\, dq_T^2\right]$$

3. Template value in bin b of reconstructed (Ω_R, q_R^2) in high statistics limit:

$$h_{X,b}(\Omega_R) = \frac{1}{\Gamma}\int w_{X,b}(\Omega_T, q_T^2)\, \epsilon(\Omega_T, q_T^2)\, M(\Omega_T, q_T^2\ |\Omega_R, q_R^2) \left[\sum_{X'} I_{X'}(q_T^2)\, f_{X'}(\Omega_T)\right] d\Omega_T\, dq_T^2\, d\Omega_R\, dq_R^2$$

Neutrino Reconstruction Procedures

Rest Frame Approximation (RFA)

Assumes that the proper velocity of the H_b hadron along the z-axis (beam axis) is the same as for the reconstructed charm–muon system (μH_c).

$$|p_{H_b}| = \frac{m_{H_b}}{m_{\mu H_c}} (p_{\mu H_c})_z \sqrt{1 + \tan^2 \alpha}$$

Quadratic Equation Solution (QDR) — Used in This Analysis

Uses the precisely known B^0 mass to estimate its momentum (up to a two-fold ambiguity) from its line of flight between the reconstructed primary and B^0 vertices.

$$|\vec{p}_{B^0}| = \frac{(m_Y^2 + m_{B^0}^2)|\vec{p}_Y| \cos\theta_{B^0,Y} \pm E_Y \sqrt{(m_{B^0}^2 - m_Y^2)^2 - 4m_{B^0}^2 |\vec{p}_Y|^2 \sin^2\theta_{B^0,Y}}}{2(E_Y^2 - |\vec{p}_Y|^2 \cos^2\theta_{B^0,Y})}$$

Across all three angles, the QDR method provides a more precise approximation of the true variables than RFA, with the most significant improvement observed in $\cos\theta_L$.

Template Fit Formalism

4. Weights:

$$w_{X,b} = \frac{f_X(\Omega_T)}{\epsilon(\Omega_T, q_T^2) \sum_{X'} \langle I_{X'} \rangle_b \, f_{X'}(\Omega_T)}, \quad \langle I_X \rangle = \frac{1}{\Gamma} \int I_X(q_T^2) \, dq_T^2$$

5. Migration matrix (2-bin example):

$$\begin{pmatrix} \langle I_q^{\text{true},1} \rangle \\ \langle I_q^{\text{true},2} \rangle \end{pmatrix} = \begin{pmatrix} M_{11} & M_{12} \\ M_{21} & M_{22} \end{pmatrix}^{-1} \begin{pmatrix} \langle I_q^1 \rangle \\ \langle I_q^2 \rangle \end{pmatrix}$$

6. Final template in bin b_1:

$$\tilde{h}_{X,b_1}(\Omega_R) = M_{11} h_{X,b_1}(\Omega_R) + M_{12} h_{X,b_2}(\Omega_R) = \int_{\Omega_T} f_X(\Omega_T) \, d\Omega_T$$

Signal templates

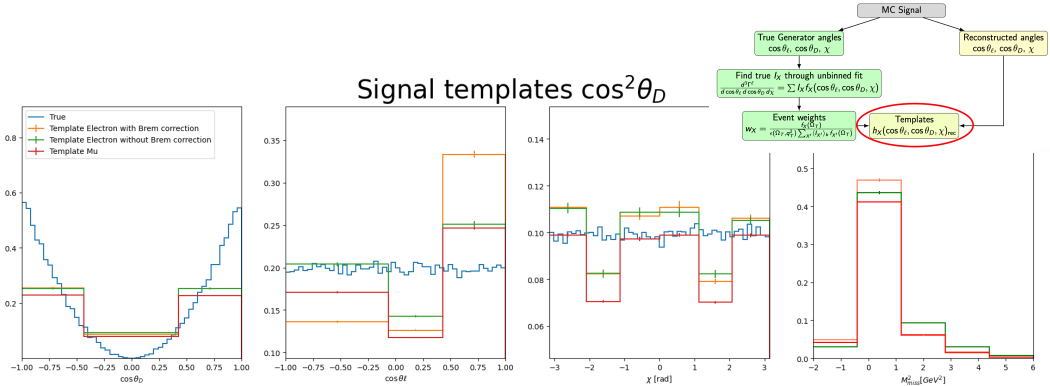

Projections on fit variables of the for one of the 12 True angular functions and corresponding templates derived from reconstructed MC events for $B^0 \to D^* \mu\nu_\mu$, $B^0 \to D^* e\nu_e$ with Brem correction and $B^0 \to D^* e\nu_e$ without Brem correction

Fit validation with bootstrapping

- To validate the fit and estimate the limited template statistics uncertainty, bootstrapping is performed on the MC sample of signal + background
- Iteration of 1000 fits reproduce generator level angles reliably
- Green vertical line - results of generator level unbinned fit
- Orange vertical line - results of signal only fit with bootstrapping

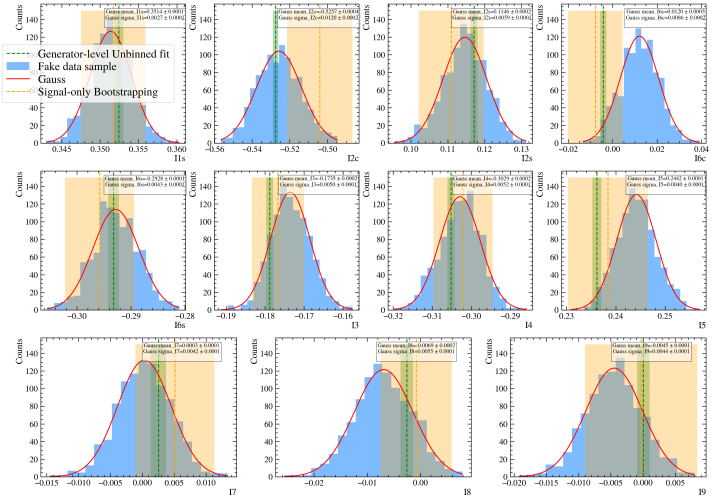

Fit validation with bootstrapping. Correlation matrix

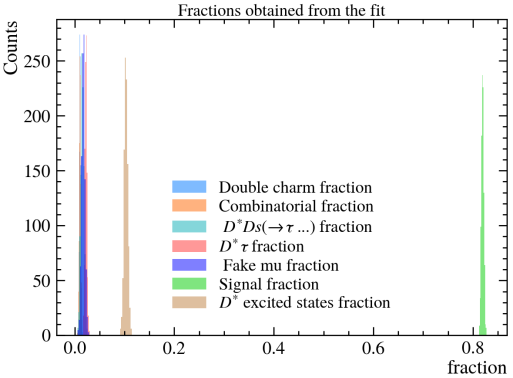

Fractions obtained from template fits with bootstrapping on Full MC

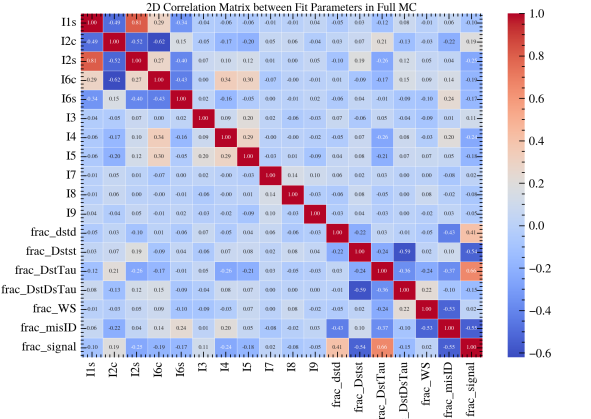

Toy studies. Toy study to assess empty bin effect

- Some of the background templates have empty bins outside of phase space restricted region
- To test the influence of background template statistics we can use the smooth density function unbinned fitting procedure that is described here: arXiv:1902.01452
- Full MC signal and density estimated background template fit of the signal and background sample
- Sampling of background templates

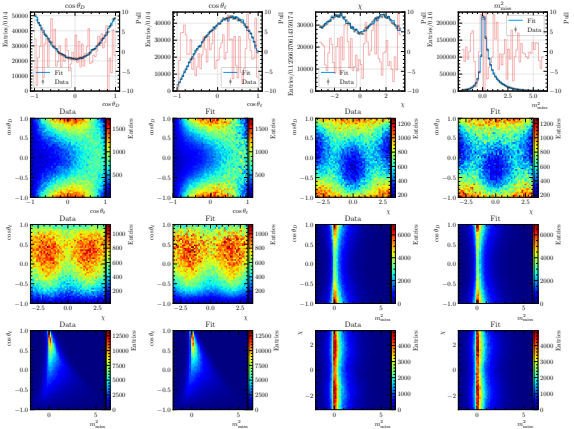

Toy studies. Toy study to assess empty bin effect. Angular coefficients

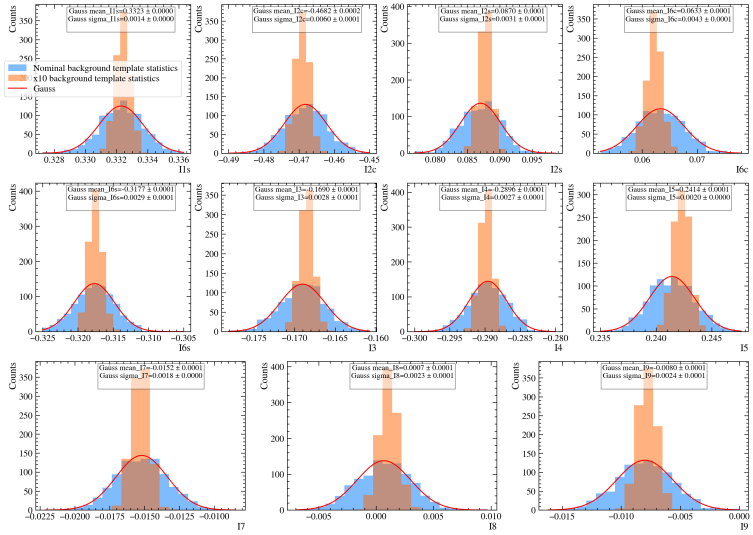

Templates

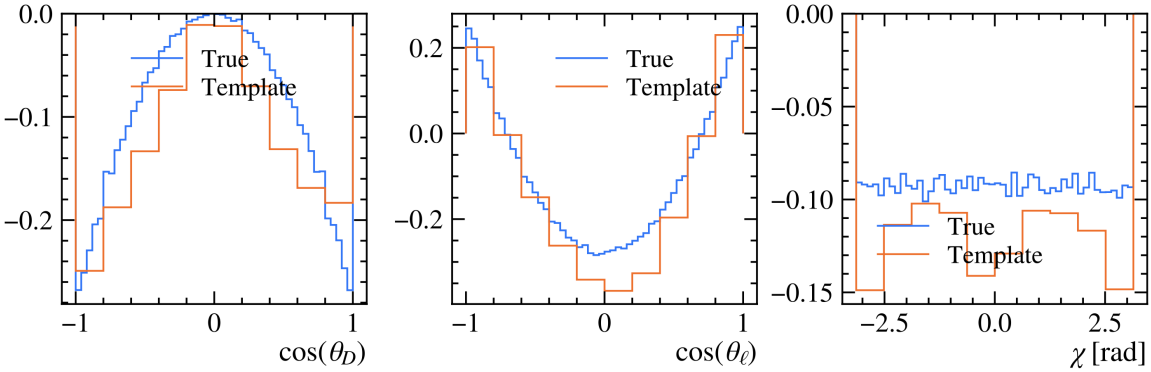

Projections for 3D template of $J_{2c}^{\mu} = \cos(\theta_D)^2 * (2.0 * \cos(\theta_L)^2 - 1.0)$ angular function

Template fit model independence

- The simplest way to prove the model Independence of 1D template fit is to remake templates with different NP contributions, i.e. to reweigh reconstructed and generator angles. If the approach is indeed model-independent, all templates are supposed to be the same within statistical uncertainty

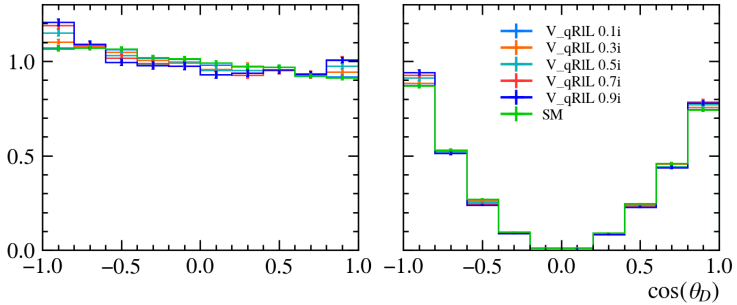

Constant template Quadratic template

Template fit cos θ_L

Template for a constant

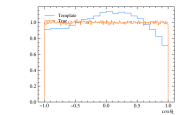

Template for a $cos\theta_L$

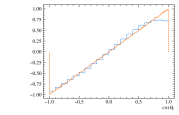

Template for a $cos^2\theta_L$

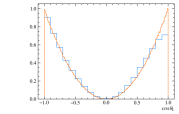

Template fit of MC with BLPR SM formfactor parametrization

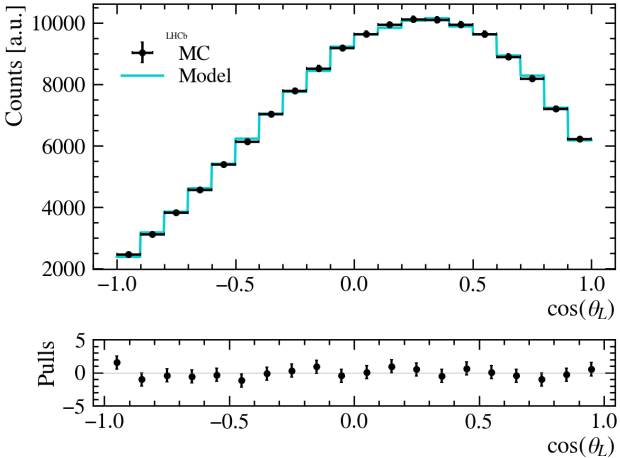

Template fit cos θ_D

Template for a constant

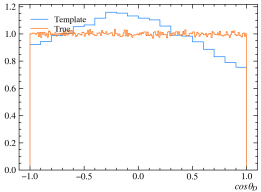

Template for a $cos^2\theta_D$

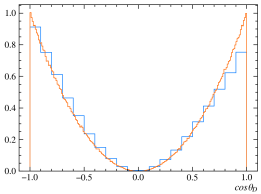

Template fit of MC with BLPR SM formfactor parametrization

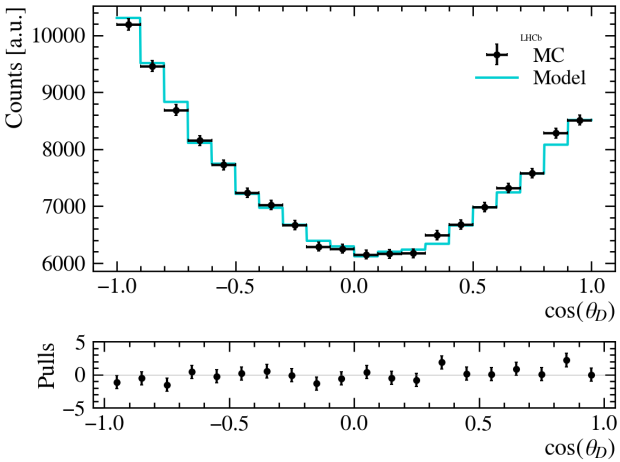

Template fit cos χ

Template for a constant

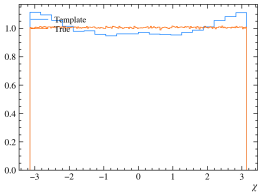

Template for a $1 + cos(2\chi)$

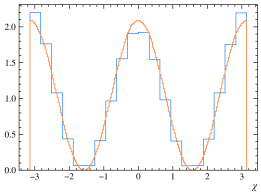

Template fit of MC with BLPR SM formfactor parametrization

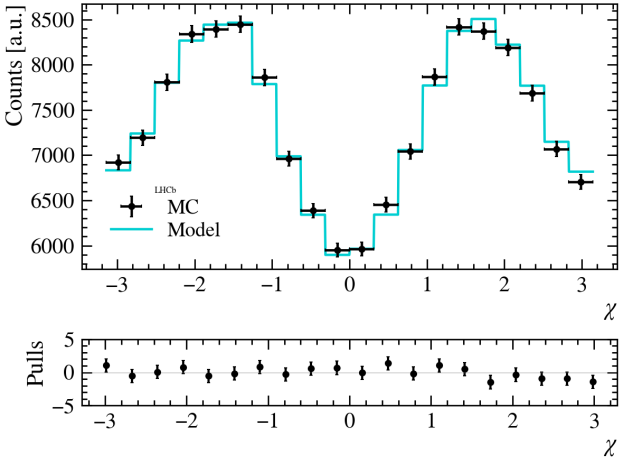

Smooth density function unbinned fitting procedure. Results

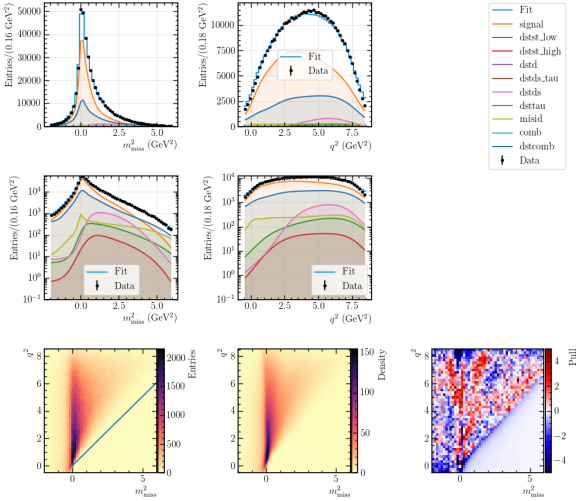

Real-time PV monitor

- The performance of the PV reconstruction algorithm heavily relies on good alignment. Therefore an additional online PV performance monitor based on two random subsets of HLT1 and HLT2 tracks was developed
- First HLT1 monitor that ran on a fraction of events in a real-time, which did not slow down the trigger throughput (new computational heavy monitors can be easily added from now on)